JGR Solid Earth

RESEARCH ARTICLE
10.1029/2025JB031278

Magmatic Volatile Flux Drives Non-Eruptive Volcano-Tectonic Seismicity at Mount St. Helens, USA From 2008–2024

Brenton W. Hirao[1], Amanda M. Thomas[1,2], David R. Shelly[3], Weston A. Thelen[4], and Cyril Journeau[1,2]

[1]Department of Earth Sciences, University of Oregon, Eugene, OR, USA, [2]Department of Earth and Planetary Sciences, University of California, Davis, CA, USA, [3]U.S. Geological Survey, Golden, CO, USA, [4]U.S. Geological Survey, Cascades Volcano Observatory, Vancouver, WA, USA

Key Points:

- Shallow, non-eruptive seismicity at Mount St. Helens is persistent between 2008 and 2024, clusters beneath the historical lava domes
- Deep seismicity becomes common after 2016 and occurs in semi-periodic swarms that last several months each
- Non-eruptive seismicity at Mount St. Helens is most likely caused by pore-pressure changes due to volatile flux from the upper-crustal magma reservoir

Supporting Information:

Supporting Information may be found in the online version of this article.

Correspondence to:

B. W. Hirao,
bhirao@uoregon.edu

Citation:

Hirao, B. W., Thomas, A. M., Shelly, D. R., Thelen, W. A., & Journeau, C. (2025). Magmatic volatile flux drives non-eruptive volcano-tectonic seismicity at Mount St. Helens, USA from 2008–2024. *Journal of Geophysical Research: Solid Earth*, *130*, e2025JB031278. https://doi.org/10.1029/2025JB031278

Received 27 JAN 2025
Accepted 19 NOV 2025

Author Contributions:

Conceptualization: Brenton W. Hirao, Amanda M. Thomas, Weston A. Thelen
Data curation: Brenton W. Hirao, Amanda M. Thomas
Formal analysis: Brenton W. Hirao, Amanda M. Thomas, Weston A. Thelen
Funding acquisition: Amanda M. Thomas
Investigation: Brenton W. Hirao, Amanda M. Thomas, Weston A. Thelen, Cyril Journeau
Methodology: Brenton W. Hirao, Amanda M. Thomas, David R. Shelly
Project administration: Amanda M. Thomas

Abstract Seismicity during non-eruptive periods is useful for observing stress changes related to magmatic transport and volatile exsolution within active volcanoes. Mount St. Helens in Washington, USA, is the most active volcano in the continental United States and has been in quiescence since 2008. To explore the processes driving seismicity at Mount St. Helens, we create a high-resolution seismicity catalog of non-eruptive seismicity from 2008 through 2023, consisting of 31,133 events. We find persistent shallow seismicity (−2.2 to 2 km below sea level (BSL), 0–4.2 km below the surface) throughout the entire study period that concentrates beneath the dacite dome complex from the 1980–1986 and 2004–2008 eruptions. Additionally, there is frequent deeper seismicity (2–8 km BSL, 4.2–12.2 km below the surface) beginning in 2016. We examine a selection of deep earthquake swarms and find complex along-depth seismicity patterns. Within swarms, increases in shallow seismicity rates can precede or are concurrent with increases of deep seismicity rates. Lastly, we discover a series of semi-periodic, shallow, burst-like swarms, consisting of low-amplitude, repetitive similar earthquakes, indicating periodic valve-like release of fluid pressure from the conduit. Increased seismic activity beginning in 2016 indicates ongoing repressurization within the magmatic system driven by recharge or crystallization-induced second boiling within the upper-crustal reservoir after 2008. The data indicate that non-eruptive seismicity at Mount St. Helens is controlled by fluid pressure changes from gas flux sourced from the magma reservoir that migrates through crack networks.

Plain Language Summary Earthquake locations and timing in volcanic settings can be used to characterize the movement of magma and gases within its plumbing system. Although the last eruption at Mount St. Helens, USA, ended in January 2008, frequent earthquakes between 2008 and 2023 indicate that it is still active. We characterize volcanic activity during the current non-eruptive period by detecting and locating over 31,000 small volcanic earthquakes, most of which are located directly beneath lava extrusion vents from two of the most recent eruptions. We find that shallow earthquakes are far more common than deep earthquakes and occur continuously throughout the study period. Deep earthquakes mostly occur within temporally clustered groups that become frequent after 2016. Lastly, we find that many shallow earthquakes are repetitive and periodic. We suggest that non-eruptive earthquakes at Mount St. Helens are caused by gas flux originating from the magma source reservoir, which increases in amplitude around 2016.

1. Introduction

Seismicity beneath active volcanoes reflects localized deformation that may be attributed to the movement of magma and its exsolved volatiles within the volcanic plumbing system (e.g., Chouet, 1996; Eaton & Murata, 1960; Klein et al., 1987; McNutt & Roman, 2015; Minakami, 1974; Roman & Cashman, 2006; Scandone & Malone, 1985; Swanson et al., 1985). Mount St. Helens, USA, is the youngest and the most active volcano in the Cascade Range volcanic arc (Decker & Decker, 1981; Gleeson, 2020; Hoblitt et al., 1980; Topinka, 2004). Since the catastrophic flank collapse and eruption of 18 May 1980, Mount St. Helens has been consistently monitored with a regional-scale seismic instrument network (University of Washington, 1963; USGS Cascades Volcano Observatory) and has become one of the most thoroughly studied volcanoes in the world. In the last four and a half decades, Mount St. Helens has experienced two seismically recorded dome-erupting sequences: the first from 1980 to 1986 (e.g., Endo et al., 1981; Lipman & Mullineaux, 1981; Swanson et al., 1985; Weaver et al., 1983) and second, from 2004 to 2008 (e.g., Dzurisin et al., 2005, 2015; Iverson et al., 2006; Moran et al., 2008; Sherrod

Resources: Amanda M. Thomas
Software: Brenton W. Hirao, David R. Shelly
Supervision: Amanda M. Thomas, David R. Shelly, Weston A. Thelen, Cyril Journeau
Validation: Brenton W. Hirao, Amanda M. Thomas, Weston A. Thelen
Visualization: Brenton W. Hirao
Writing – original draft: Brenton W. Hirao, Amanda M. Thomas
Writing – review & editing: Brenton W. Hirao, Amanda M. Thomas, David R. Shelly, Weston A. Thelen, Cyril Journeau

et al., 2008). In addition, a series of phreatic eruptions were observed from 1989 to 1991 (Mastin, 1994). Sixteen years have passed since the end of the last eruption in January 2008, providing a unique opportunity to examine trends in seismicity and its evolution after a long-lived dome-building eruption (K. V. Cashman et al., 2008; Pallister et al., 2013) and how they reflect changes of a dacitic volcanic plumbing complex in the upper crust (K. V. Cashman et al., 2017).

1.1. Upper Crustal Volcanic Structure

Melt within the Cascade volcanic arc is sourced from below the Moho discontinuity at 35–40 km below sea level (BSL) (e.g., Kiser et al., 2016, 2021; Stanley et al., 1990). It is then transported toward the upper-crustal volcanic complex at Mount St. Helens through a vertically extensive transcrustal magmatic system (Bedrosian et al., 2018; K. V. Cashman et al., 2017; Kiser et al., 2016, 2021; Leeman & Smith, 2018; Smith & Leeman, 1993; Wanke et al., 2019, etc.) Mount St. Helens is positioned above the St. Helens Seismic Zone (SHZ, Figure S1a in Supporting Information S1), a NNW–SSE oriented strike-slip fault zone that facilitates the transfer of magma toward the upper-crustal reservoir (Lehto et al., 2013; Musumeci et al., 2002; Weaver et al., 1983). Numerous constraints from petrologic (K. Cashman & Blundy, 2000; K. V. Cashman & McConnell, 2005; Pallister et al., 1992, 2008; Rutherford & Hill, 1993), geodetic (Anderson et al., 2010; Anderson & Segall, 2011, 2013; Scandone & Malone, 1985; Wong et al., 2017; Wong & Segall, 2019, 2020), and tomographic studies (De Siena et al., 2014; Kiser et al., 2018, 2019; Lees, 1992; Ulberg et al., 2020; Waite & Moran, 2009) agree that the upper extent of the shallow crustal magma reservoir lies between 5 and 8 km BSL, or between 7 and 10 km directly beneath the crater floor of Mount St. Helens. Magma from the source reservoir is transported to the crater floor during eruptions through a narrow, vertical conduit (Pallister et al., 2008, 2013). In addition, field observations conducted after the 2004 to 2008 eruption reveal that the upper 0.5–1 km of the conduit is filled with a solidified dacite plug with low porosity and volatile content (K. V. Cashman et al., 2008; Gaunt et al., 2014, 2016; Heap et al., 2016; Pallister et al., 2013).

1.2. Seismicity During Non-Eruptive Periods

The location, timing, and character of seismicity are useful for observing magmatic and volatile transport processes that occur during non-eruptive periods. Seismic events at Mount St. Helens are routinely identified, located, and published in an event catalog by the Pacific Northwest Seismic Network (PNSN) (University of Washington, 1963). Multiple types of volcanic seismicity have been identified at Mount St. Helens, including volcano-tectonic (VT) earthquakes (Moran, 1994; Moran et al., 2008; Thelen et al., 2011), long-period (LP) earthquakes (Fehler & Chouet, 1982; Glasgow et al., 2018; Han et al., 2018; Hansen & Schmandt, 2015; Matoza & Chouet, 2010; Matoza et al., 2015; Nichols et al., 2011; Vidale et al., 2014; Waite et al., 2008), and tremor (Denlinger & Moran, 2014; Fehler, 1983; Köpfli et al., 2024; Malone, 2020; Moran et al., 2008). VT earthquakes, which are characterized by a waveform character and frequency spectra that resemble an earthquake from a tectonic source (e.g., Endo et al., 1981; Malone et al., 1983; Power et al., 1994; Stephens et al., 1994), are the most commonly recorded seismic event type during non-eruptive periods (Glasgow et al., 2018; Lehto et al., 2013; Moran et al., 2008).

VT seismicity during non-eruptive periods at Mount St. Helens is typically attributed to slip on pre-existing faults triggered by pore-pressure variations (Benson et al., 2008; Goto, 1999; Scholz, 2019; Tuffen et al., 2008) in crystallized magma or wallrock. These variations, thought to be due to magmatic volatiles and fluids that originate from the upper crustal magma chamber, are then channeled to shallower depths through the conduit (Moran, 1994; Moran et al., 2008; Musumeci et al., 2002; Zhang et al., 2022). Shallow VT activity between −2 and 2 km BSL is common and persistent during the non-eruptive periods from 1992 to 2004 and 2008 to 2023. By contrast, VT earthquakes deeper than 2 km tend to cluster within quasi-periodic swarms that last from several months to several years and are regarded as evidence for repressurization induced by magmatic recharge (Moran, 1994; Moran et al., 2008; Musumeci et al., 2002; Zhang et al., 2022). Lastly, VT earthquakes can occur adjacent to an upper crustal magma reservoir below roughly 8 km BSL, but rarely occur within it (Lehto et al., 2013; Moran, 1994; Moran et al., 2008; Musumeci et al., 2002; Zhang et al., 2022). In this study, we use an augmented seismicity catalog to observe spatial and temporal patterns in VT seismicity, from which we infer the locations of brittle structures, mechanisms of volatile transfer, as well as the evolving state of pressurization during the current non-eruptive period.

2. Methods and Data

We create an enhanced, high-resolution seismicity catalog with the goal of observing the evolution of non-eruptive seismicity between January 2008 and the end of December 2023 (Video 4, Data S1, 10.5281/zenodo.17089016). We detect and locate both previously cataloged and newly discovered events by applying a network-based template-matching and location workflow similar to Shelly et al. (2013, 2016) and Ross et al. (2019), using multi-station P- and S- waveform templates from a total of 4,044 analyst-identified events recorded between January 2008 and December 2023 (University of Washington, 1963). We apply this workflow to a total of 57 short period broadband seismometers within approximately 50 km of the Mount St. Helens edifice. Station metadata may be viewed in Text S5 in Supporting Information S1 and Table S1. In this section, we summarize the key components to the detection and location workflow and provide additional details concerning data quality selection and location uncertainty estimation in Text S1 and S2 in Supporting Information S1.

2.1. Event Location: Three-Dimensional Velocity Model

Accurately locating earthquakes at Mount St. Helens is challenging owing to its complex velocity structure and high topographic relief, which can influence seismic ray paths and travel times over typical source to receiver length scales (Burjánek et al., 2014; Neuberg & Pointer, 2000; Ripperger et al., 2003; Zhang et al., 2022). To mitigate these effects, we use the three-dimensional (3D) P- and S-wave velocity models of Kiser et al. (2019). These models were derived from the recordings of active source borehole shots on over 3000 geophones during the Imaging Under Mount St. Helens (iMUSH) dense array experiment in 2014 (Kiser et al., 2016, 2019). We then resolve 3D P- and S-wave travel time grids using "Stingray," a seismic ray tracing algorithm from Moser (1991) and Toomey et al. (1994). In addition, we input into Stingray the 15 s topographic model from the NASA Shuttle Radar Topography Mission (SRTM, 2013). The resulting grids are centered at the middle of the Mount St. Helens crater at −122.19° longitude and 46.20° latitude, span 100 km along longitude (x), 95 km along latitude (y), and 40 km below the topographic surface (z), and have a spacing of 0.25 km. We use these grids to solve for absolute and relative locations in NonLinLoc (Lomax et al., 2000, 2014) and GrowClust3D (Trugman et al., 2023; Trugman & Shearer, 2017), respectively.

2.2. Event Detection: Template Matching

Network-based template matching is well suited for detecting low amplitude events in volcanic environments (Garza-Giron et al., 2023; Hotovec-Ellis et al., 2018; Matoza et al., 2015; Shelly et al., 2013, 2016). Each template is associated with a starting location that is solved using analyst-confirmed phase arrivals with the NonLinLoc OCT-TREE nested grid search algorithm (Lomax et al., 2014). We then generate separate 2.5-s-long waveform templates for P- and S-wave arrivals for each station used to record the template, including all available channels. Each waveform template begins 0.5 s before its respective arrival time. We predict the arrival time of missing S-wave arrival picks using a Vp/Vs ratio of 1.65. If the difference between S- and P-wave arrivals is less than 2.5 s, the P-wave template is truncated to exclude the S-wave arrival. Continuous waveform streams are loaded and pre-processed using tools included in Obspy, a Python library for processing seismological data (Beyreuther et al., 2010). Prior to cross-correlation, we detrend, taper, interpolate to 100 Hz, and filter each template and day-long waveform trace with a zero-phase Butterworth filter between 2 and 20 Hz.

Each template is cross-correlated with continuous seismic data on all days that have at least 4 available stations within the template between January 2008 to December 2023. Day-long normalized cross-correlation (NCC) functions generated with the Super Efficient Cross- Correlation package (Senobari et al., 2019) are then summed across all channels and phases from the template. An event detection is considered when peaks of the summed NCC function exceed 12 times its median absolute deviation. We choose the 12*MAD threshold after Ross et al. (2019) to favor detection robustness over long time periods where station health and noise can vary significantly. The resulting cross-correlation and differential time measurements are input into the GrowClust3D algorithm (Trugman et al., 2023), which simultaneously locates newly detected events and relocates cataloged template locations. Our resulting catalog contains 31,133 events (about 7.7 times greater than the PNSN catalog) with magnitudes between −3 and 4.5 (Figure S3 in Supporting Information S1) within a roughly 4 km radius of the middle of the Mount St. Helens edifice.

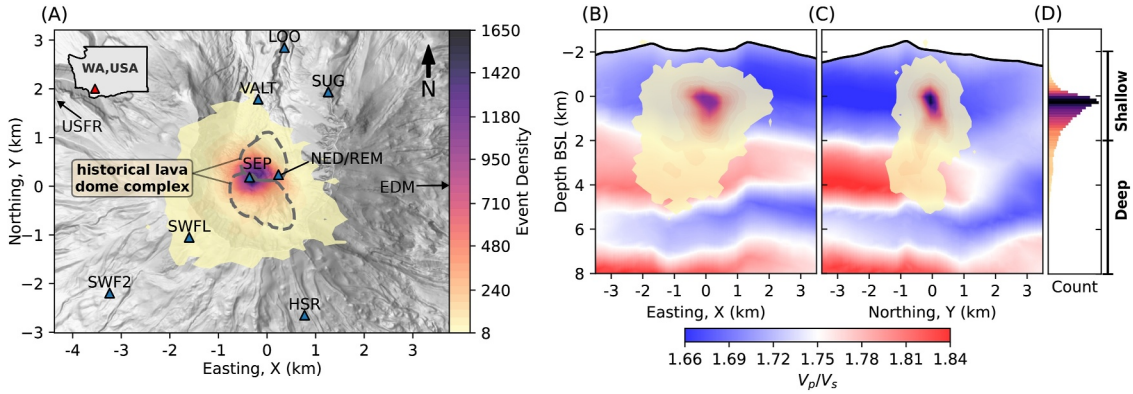

Figure 1. (a) Mount St. Helens, Washington, USA, study area projected along easting and northing in map view. Event density is depicted with contours, stations near the edifice are in triangles, and dashed outline shows boundaries of the historical dome complex. North of station SEP are lava domes from the 1980–1986 eruptions. South of station SEP are the 2004–2008 lava spines. Outlines of the lava dome complex are modified from Major et al. (2005) and Gabrielli et al. (2020). Stations USFR and EDM are nearby but outside of the map boundaries. Earthquake density contours are drawn from roughly 0.2 km by 0.2 km (0.04 km^2) bins. Contours from bins containing at least 10 events each from the enhanced catalog in 2008–2024 in cross section along Easting (b), and Northing (c) superimposed on the *Vp*/*Vs* model from Kiser et al. (2019) velocity model, which we use for locating earthquakes in this study. Depth/*X*, *Y* aspect ratio in (b) and (c) is 0.7. Normalized earthquake depth histogram shown in (d). Full station configuration is shown in Figure S1 in Supporting Information S1. Topographic profiles in (b) and (c) are interpolated from SRTM (2013) at $X = 0$, and $Y = 0$, respectively.

2.3. Event Magnitudes

We measure the size of both previously cataloged events and new events using the relative magnitude procedure described by Shelly et al. (2016). To reconcile changes in template event location and derive magnitudes for template events with a consistent scale, we compute the Richter magnitude (ML) using the Obspy estimate_magnitude function (Beyreuther et al., 2010) and attenuation-correction terms of Bakun and Joyner (1984). The resulting ML values are then extended to new events by computing the relative amplitude method of Shelly et al. (2016). Here, we refer to the extended local magnitudes as ML_ext. Additional details for the magnitude computation procedure are described in Text S4 in Supporting Information S1.

2.4. Changes to Monitoring Network and Magnitude of Completeness Correction

Within 10 km of the modern-day crater floor, a total of 6 stations (CC.NFT, CC.HOA, CC.USFR, CC.REM, CC.SWF2, CC.LOO) were added and 3 stations (CC.SWFL, CC.NED, UW.JUN) were removed (Figure 1a, Figure S1 in Supporting Information S1). Changes in the quantity of broadband stations near Mount St. Helens throughout the 2008 to 2023 study period can influence the ability of the network to detect and locate small magnitude events. Thus, changes in apparent event rate may reflect changes in the seismic network detection threshold, instead of true changes in seismic activity. To ensure a robust interpretation of long-term event rates, we apply a time-dependent magnitude of completeness correction within non-overlapping time windows. To test the effect of window length on completeness magnitudes (Mc), we compute Mc within 3-month, 6-month, 1-year, and 2-year long windows. For each window, we compute the frequency-magnitude distribution with 0.1 magnitude-wide bins and estimate the completeness magnitude of each window using the maximum curvature (MAXC) definition of Wiemer and Wyss (2000). Here, the Mc is equated to the magnitude bin with the highest frequency. We choose the MAXC definition because it is simple to compute and does not require assumed b-values (Lapins, 2022). To balance between temporal resolution and numerical stability, we apply the time-dependent Mc computed within 6-month long bins. We apply the Mc to the long-term event rates by removing events that are below the Mc at its respective time (Figure S2 in Supporting Information S1). Trends in both the uncorrected and Mc corrected seismicity rates closely resemble each other. Thus, analysis and discussion of event-rates presented in this manuscript are based on the uncorrected rates computed with all events in the catalog.

2.5. Moment Tensor Solutions

We attempt to constrain source mechanisms for individual earthquakes in the PNSN catalog using the MTfit package, which probabilistically solves for both full moment tensors and double-couple solutions using first-

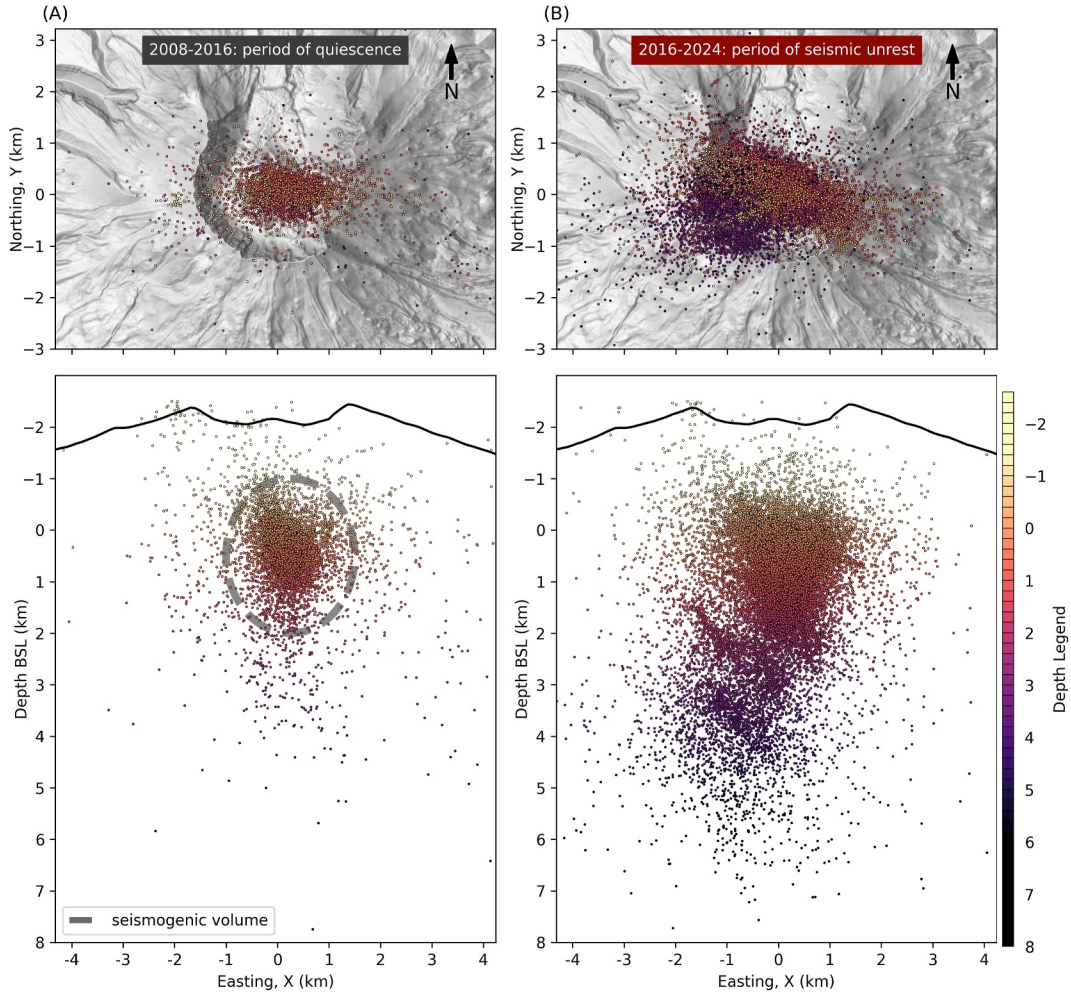

Figure 2. Map and depth sections of seismicity within the periods (a) 2008 to 2016 and (b) 2016 to 2024 (see Figure 3). Seismogenic volume is drawn in (a).

motion P-wave polarities (Mildon et al., 2016; Pugh & White, 2018). We analyze a selection of 31 well-recorded earthquakes with good focal sphere coverage and at least 15 analyst-picked polarities, which are accessed through Obspy (Beyreuther et al., 2010) from the IRIS database. Special care was taken to correct for inverted vertical channel orientations at some recording stations, according to the IRIS metadata. We choose not to use P- S amplitude ratios as we do not have empirical station correction terms to accommodate the heterogeneous site effects (e.g., Hardebeck & Shearer, 2003). We then solve for source-to-station azimuth and takeoff-angle grids using the NonLinLoc Time2Angles function, which are then interpolated for their precise location determined from the template match and relative location procedure. The polarities and maximum likelihood solutions for full moment tensor and double-couple inversions are shown in Figures S9–S11 in Supporting Information S1.

3. Results

3.1. Spatial Patterns

Most seismicity within our catalog is laterally confined within a 2-km radius centered near the middle of the 1980s crater floor (Figures 1a and 2a). The distribution of earthquake epicenter density sharply concentrates toward the middle of this source region, which lies beneath remnants of the dacite lava domes and spines extruded during the 1980 to 1986 (e.g., Lipman et al., 1981) and 2004 to 2008 (e.g., K. V. Cashman et al., 2008; Pallister et al., 2013) eruptive periods, respectively. Nearly all seismicity within our catalog occurs at depths between the crater floor and around 7.5 km BSL, with the lower limit of seismicity roughly consistent with the upper extent of the

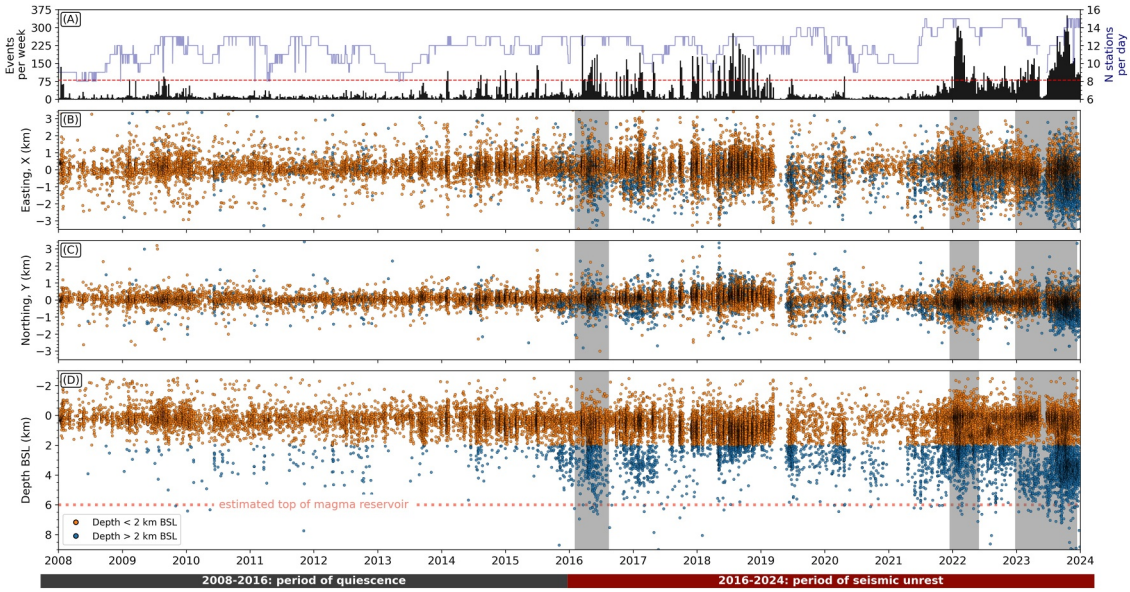

Figure 3. (a) Weekly earthquake rates (black histograms) and number of stations per day within 10 km of the edifice (blue line). Dashed red line in (a) depicts the 80 event per week rate threshold dividing earthquake swarm and background rate ranges. Individual days with fewer than 7 operating stations were removed to emphasize long term trends in station count. (b, c, and d) Earthquake locations along *X*, Y, and depth below sea level (BSL) for entire 2008 to 2024 study period. Earthquakes shallower than 2 km BSL and deeper than 2 km BSL are colored orange and blue, respectively. The estimated top of the magma reservoir (red dotted line in d) is constrained from numerous seismic, petrologic, geodetic, and tomographic studies listed in the Introduction. Light gray patches are swarms examined in Figures 4a–4c. See Video S4 for animation of the entire time series. See Section 3.1 for discussion regarding depth datum and the boundary between "shallow" and "deep" seismicity depth ranges.

magmatic source reservoir. For convenience, we refer to depth regions between the crater floor (−2.2 km BSL) to 2 km depth BSL as "shallow," and 2–8 km depth BSL as "deep." The boundaries we define here are not to be confused with those defined by other studies, which may include: 2–3 km below a datum at 1.1 km above sea level (ASL) in Moran (1994) and Moran et al. (2008), 0.5 km BSL in Zhang et al. (2022), 3 km below a 2.2 km ASL datum in Lehto et al. (2010, 2013), and 2 km below the surface in Waite et al. (2008). Approximately 87% of all hypocenters occur at depths shallower than 2 km BSL (Figure 1d) (25,855 shallow and 5,278 deep earthquakes). Most shallow earthquakes localize within a distinct seismogenic volume of roughly 1 km radius area between −0.5 and 2 km depth BSL (Figures 1b–1d). In further discussion we refer to this shallow zone as the "seismogenic volume" (Figure 2a). Similar groups of persistent shallow earthquakes have also been previously identified between 1991 and 2004 and after 2008, which have been referred to as a shallow "seismogenic volume," "seismicity band," or "seismic lid" (Lehto et al., 2013; Moran et al., 2008; Zhang et al., 2022).

The uncertainties of deep earthquake locations are nearly twice as large as uncertainties for shallow earthquakes (Figure S5 in Supporting Information S1). In addition, all earthquakes have location uncertainties that are twice as great along the east-west direction as along the north-south direction, owing to the station geometry near the edifice (Figure 1a, Figure S1 in Supporting Information S1). The median one standard deviation uncertainties along east-west (*X*), north-south (*Y*), and depth are 0.66, 0.32, and 0.59 km for shallow earthquakes and 1.01, 0.52, and 1.05 km for deep earthquakes. This may partly explain why deep earthquakes are more spatially diffuse than shallow earthquakes, and why hypocenters occupy a wider footprint along the east-west direction compared to the north-south direction (Figures 1–3).

3.2. Long Timescale Patterns

We divide the study period into two distinct eight-year-long periods from 2008 through the end of 2015 and from 2016 to 2024, which we refer to as the "period of quiescence" and the "period of seismic unrest," respectively (Figures 2 and 3). These two eight year-long periods are distinguished by the relative absence and abundance of deep seismicity, respectively. Shallow seismicity within and around the seismogenic volume (depth <2 km BSL) is persistent throughout the entire 2008 to 2023 study period (Figure 3d). Deep seismicity is rare between 2008 and 2016 but is frequent between 2016 and 2024, where it usually clusters within earthquake swarms that each last

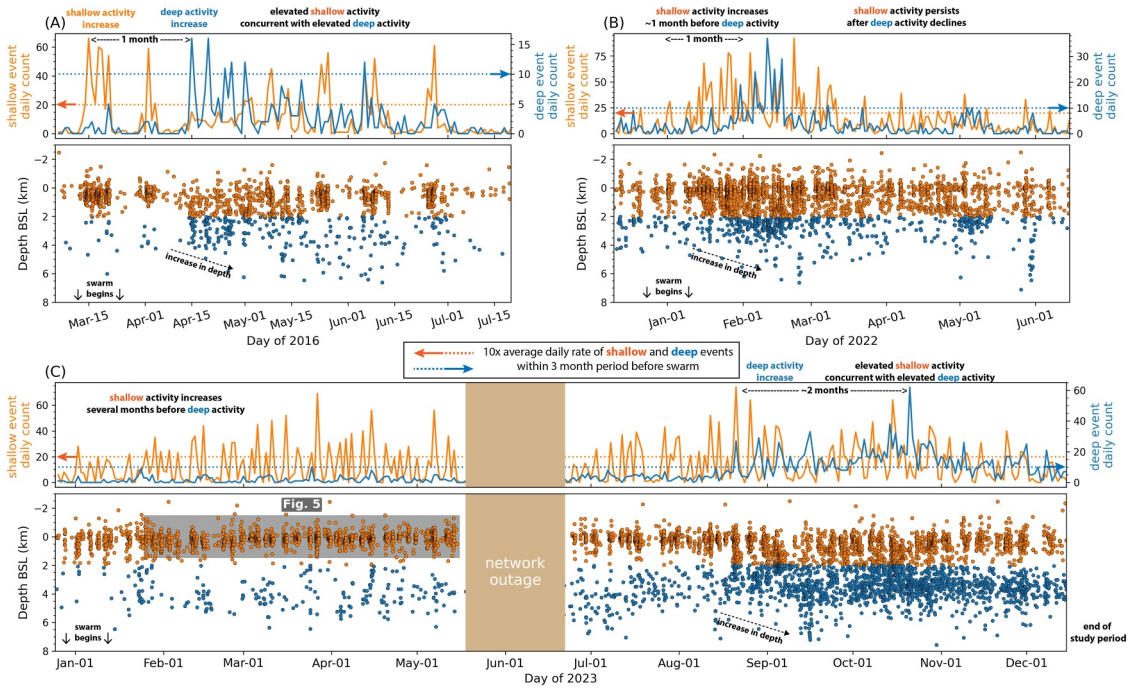

Figure 4. Earthquake swarms shown in gray patches from Figure 3. (a) 2016, (b) early 2022, and (c) 2023 (c). Shallow and deep earthquake daily rates are shown in each top panel on left and right-side axes, respectively. The horizontal dotted lines show the equivalent of 10 times the average daily rate of shallow and deep events within a 3 month period before each swarm started. Earthquake depths plotted against time on bottom axes. See Videos 2–4 for four-dimensional depictions of these swarms.

several months (Figure 4). The number of broadband seismic recording stations within 10 km of the edifice increases from 8 to 15 between 2008 and 2023, with temporary decreases in station count due to poor weather in the winter months (Figure 1a). For discussion, we arbitrarily define an earthquake "swarm" as a continuous or near continuous period where the earthquake rate exceeds a "background rate" threshold of 80 events within a one-week bin (Figure 3a, Figure S2 in Supporting Information S1). Our choice of 80 events per week is to distinguish periods of relatively high or low event rates and does not reflect a criterion defined by previous studies. The long-term changes in event rates discussed here closely resemble those corrected for by the time-dependent magnitude of completeness (Figure S2 in Supporting Information S1), which suggests that they reflect true changes in seismic activity at Mount St. Helens.

The period of quiescence begins in January 2008, during the final weeks of the 2004–2008 eruption (Dzurisin, 2018; Dzurisin et al., 2015). Small shallow swarms in early January mark the final stages of the eruption, after which seismicity drops to fewer than 10–30 events per week. Over the next eight years, activity is dominated by low-rate shallow seismicity near the seismogenic volume (Figure 2a), occasional deep events, and weak inflation (Figures 3a–3d; Figure 2a; Figure S4b in Supporting Information S1; Dzurisin et al., 2015). A small number of shallow swarms occur in January 2008 (Figure S5a in Supporting Information S1) and August–September 2009 (Figure S5b in Supporting Information S1), after which, seismicity rates remain low. Semi-periodic shallow swarms reappear in mid-2013, July–October 2014, and July 2015, with weekly rates peaking at 100–150 events (Figure 3a; Figure S2c in Supporting Information S1).

Beginning in 2016, the period of seismic unrest hosts several recurring earthquake swarms with relative increases in earthquake activity at shallow (less than 2 km BSL) and deep (2–8 km BSL) depth ranges. The years 2016, 2017, and 2018 each featured several swarms per year where seismic event rates reached 100 to 200 events per week, before decaying to background rates between 2019 and late 2021. The final two years of the study period, 2022 and 2023, feature the highest peak and persistent seismic activity levels in the entire study period. In 2022 and 2023, seismicity rates reached as high as 240 to 350 events per week.

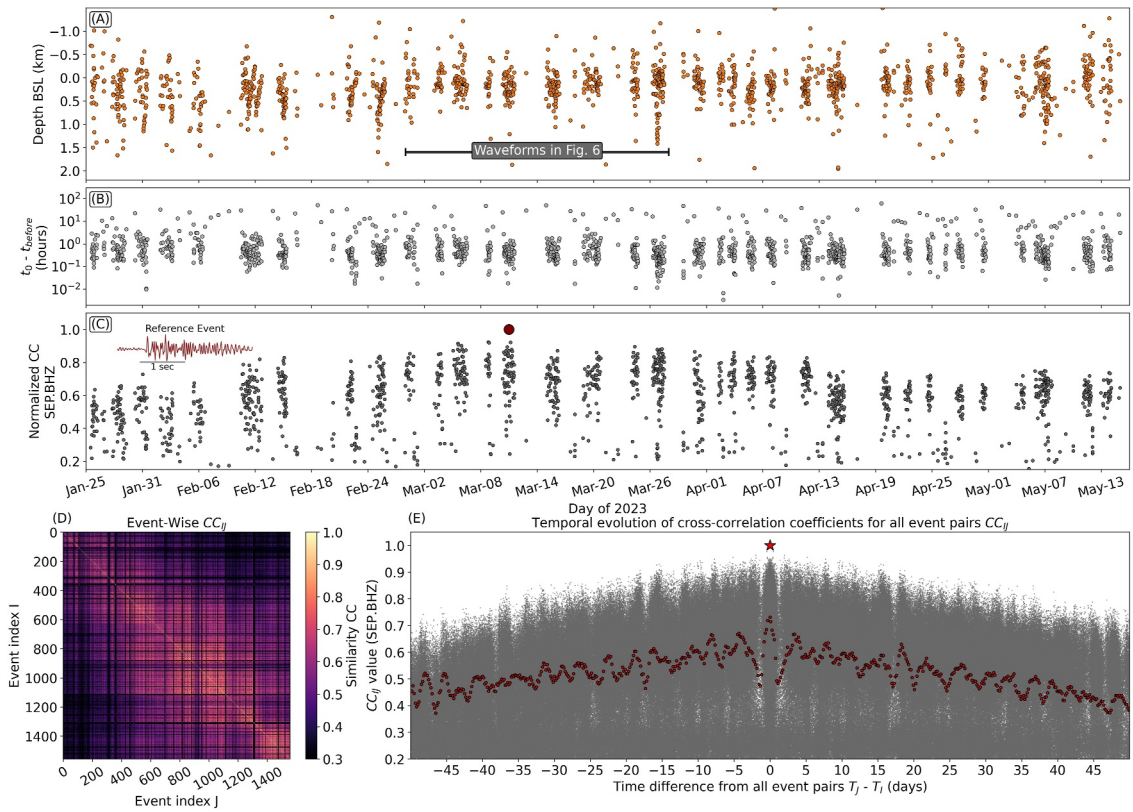

Figure 5. Shallow seismicity bursts between January and May 2023, from Figure 4c. Time series of (a) depths, (b) recurrence intervals, and (c) cross-correlation coefficients of all events in this period with respect to a reference event (dark red dot in c) on 11 March 2023. (d) Event-wise cross-correlation matrix. (e) Change in event-wise cross-correlation values (gray dots) for all events with respect to any reference event (red star) event in (a) plotted versus the relative time difference in each event pair. This graph shows the same information as (d) but is projected with respect to the event pair time difference. Red dots are the mean values for each four-hour long bin. See Figure S7 in Supporting Information S1 for a detailed inspection of inter-event cross-correlation values of P-S and coda phases.

3.3. Swarms: Shallow and Deep Event Timing

We explore the evolution of along-depth seismicity distributions over several-month-long timescales by examining the relative timing between shallow and deep earthquake daily event counts for three well-recorded swarms in March–July 2016, January–June 2022, and January–December 2023 (Figures 4a–4c, Videos S2–S4). All three examples show that shallow and deep event activity rates within earthquake swarms are temporally concurrent (Figures 4a–4c). In all three cases, the number of shallow and deep event rates per day both far exceed 10 times the average rates of a three-month period leading up to each respective swarm.

In general, event rate increases of shallow seismicity can either precede those of deep seismicity by several weeks or occur at roughly the same time. During swarms, increased deep earthquake activity can persist continuously for several weeks to months. In addition, shallow seismicity rates remain elevated throughout periods of increased deep event activity. Shallow seismicity earthquake rates can decay concurrently with those of deep earthquakes or persist for several weeks after the rate of deep events has declined to pre-swarm levels. Continuous migration fronts are rarely observed. Instead, most seismicity occurs within burst-like clusters with complex short-term migrations that collectively move along depth over several-week-long timescales. We choose not to interpret individual small-scale migration patterns as individual geologic structures, since this would require rigorous location precision testing to ensure robustness (J. Battaglia et al., 2004; Thelen et al., 2011) The 2016 swarm (Figure 4a, Video 2) features bursts of up to 60 shallow earthquakes per day, which precede the onset of near continuous deep activity by two to four weeks. As many as 60 shallow and 15 deep earthquakes per day were recorded between 15 April and 1 July2016, before decaying to background activity rates. Similarly, the 2022 swarm (Figure 4b, Video 3) consists of shallow event rate increases that begin about four weeks before the onset of deep seismicity rate increase. Up to 80 shallow and 20 deep earthquakes per day were recorded between 1

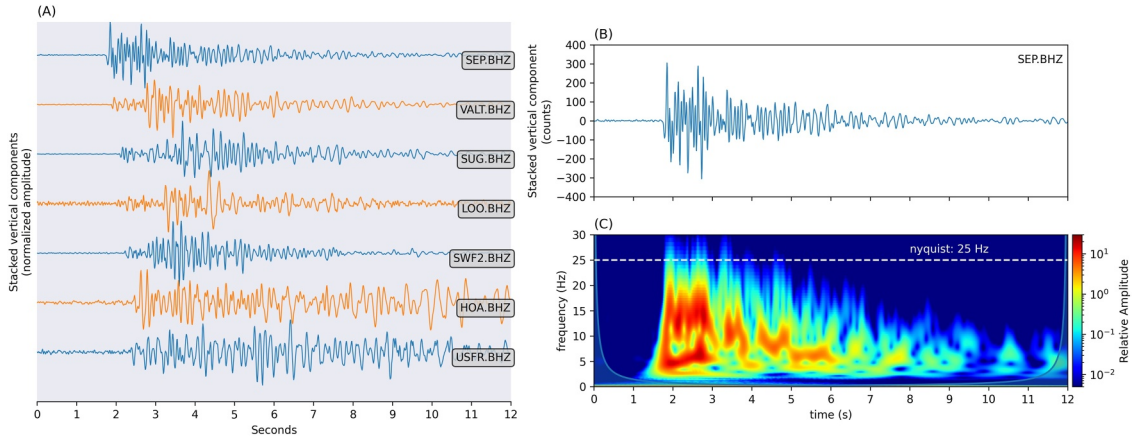

Figure 6. (a) Multistation waveform stack containing 300 shallow burst events from February to April 2023, shown in Figure 5a. (b) continuous wavelet transform spectrogram (c) of stack from the SEP.BHZ channel.

January and 1 April 2022. A small, isolated cluster of around 60 earthquakes between 2 and 3 km depth occur between 1 May and 15 May. An average of 50 earthquakes per week are recorded between June 2022 until the start of the third swarm in July 2023—significantly greater than rates observed during most of the 2008 to 2016 quiescent period.

The mid to late 2023 swarm (Figure 4c, Video 4) features the largest number of earthquakes and is the most long-lived swarm that we discuss in this section. Heightened seismicity rates during this period were originally reported by the Cascades Volcano Observatory (2023). A portion of this swarm is hidden by a network-wide service outage between May and June 2023. Like the 2016 and 2022 swarms, increases in deep seismicity rate occur after increases in shallow activity rates. However, higher-than-average levels of persistent shallow and deep seismicity started shortly after the end of the January–June 2022 swarm. Between 20 and 70 shallow and 10 to 50 deep earthquakes were consistently recorded per day between mid- August until the end of December 2023. This swarm may extend into 2024, beyond the end of the study period.

3.4. Shallow Burst-Like Swarms

A close inspection of shallow seismicity during the 2016, 2022, and 2023 swarms indicates that many shallow earthquakes occur in quasi-periodic 'burst-like' clusters, which we refer to as "shallow seismicity bursts" (also referred to as "bursts"). We focus on a well-recorded sequence of shallow bursts from late-January to mid-May 2023 for in-depth analysis (Figures 4c, 5, and 6). The events within shallow seismicity bursts during this period are concentrated in a compact source volume between −0.5 and 1 km BSL (Figure 5a), located in the shallow seismogenic volume (Figures 1, 2a, and 7). The timing and recurrence intervals (Figure 5b) show that each shallow burst lasts from one to two days in duration, recurs between one to four days of each other, and contains between 5 and 30 shallow earthquakes.

We explore inter-event waveform similarity for all shallow earthquakes within this period by computing the event-wise cross-correlation coefficient for every event pair recorded on the vertical EHZ channel of station SEP, as it is the nearest station to the source region. Prior to event-wise cross-correlation, the waveform of each event is trimmed to 4 s in duration beginning 0.5 s before the expected P-wave arrival, interpolated to 100 Hz, and high-pass filtered above 1 Hz. We show the resulting inter-event cross-correlation between a reference event on 11 March 2023 (referred to as T0) in Figure 5c and the full inter-event cross-correlation matrix (CCij) in Figure 5d. The inter-event cross correlation indicates a steady increase in waveform similarity from no greater than 0.65 in late January 2023 to roughly 0.9, a few hours before T0, followed by a decline at a similar rate until mid-May. The progressive increase and decrease of mutual waveform similarity is a common feature among several events within shallow bursts between January and May 2023 (Figures 5d and 5e). To investigate whether the long-term change in inter-event cross-correlation is caused by an evolution in the location, source mechanism, or path, we separate the waveforms into two sections--the first containing body wave or P- and S-wave arrivals and second containing coda phases (Figure S7 in Supporting Information S1). We then compute the inter-event cross-

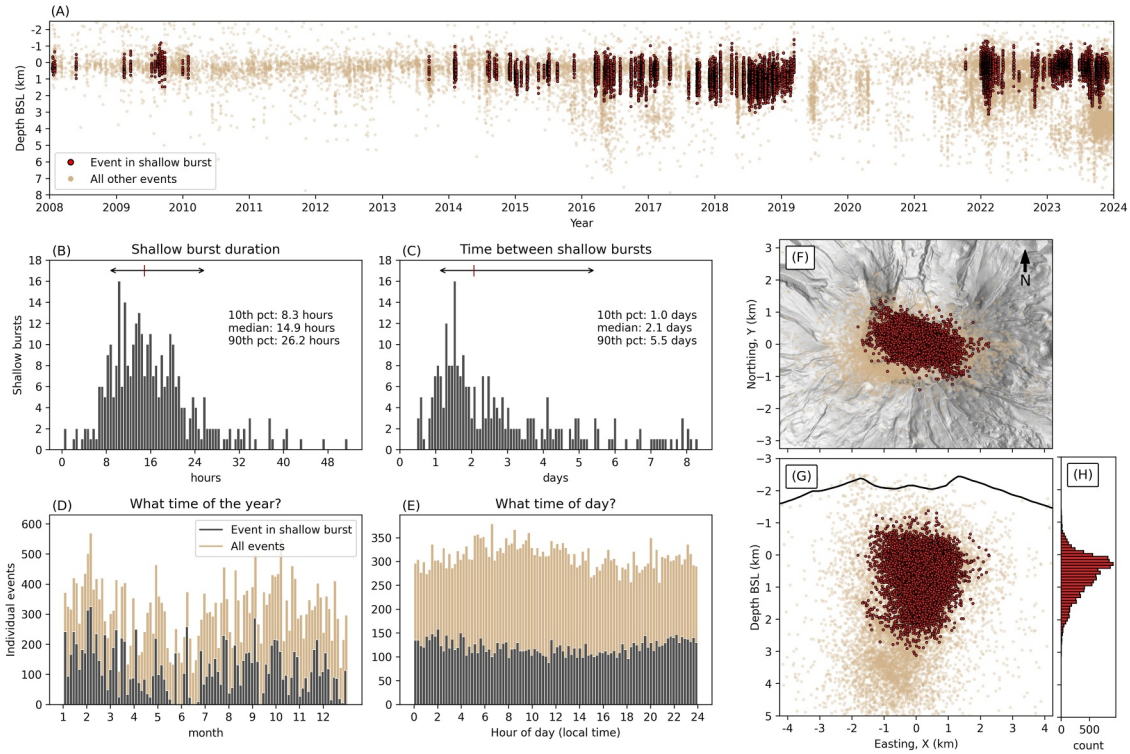

Figure 7. (a) Depth time series between 2008 and 2024 showing all detected shallow bursts using ST-DBSCAN. (b) and (c) are histograms showing distributions of durations of and time between individual shallow bursts within their respective sequences. Shallow bursts that are more than 8 days apart from each other are not a part of the same sequence. Horizontal arrow and red tick show the 10th to 90th percentiles and median values. (d) and (e) show distributions of month and hour of day for all individual events within shallow bursts and the entire data set. Location of shallow burst events in map view (f), along depth (g), and depth distribution (h).

correlation for both sections independently. Most of the body wave inter-event cross-correlation values are between 0.75 and 1, suggesting a high degree of similarity with a slight increase leading to the reference event and slight decrease afterward (Figures S7a, S7d in Supporting Information S1). By contrast, the evolution of inter-event coda phase cross-correlation coefficients closely resembles the trends observed in those of whole waveform inter-event cross-correlation values (Figures 5c–5e). Inspection of the aligned waveforms shows a consistent first-motion polarity.

Individual events within shallow bursts are of low signal to noise, however their near-repetitive waveform character makes it possible to stack and characterize several hundred similar events. We align and compute the NCC-weighted average of 300 events from this sequence to form a characteristic multi-station waveform stack (Figure 6a). We then compute the continuous wavelet transform spectrogram (Figure 6c) for the stacked waveform on SEP.EHZ (Figure 6b), as it is the nearest station to the event source region. CWT analysis of the SEP.EHZ waveform stack shows that it is rich in coherent 2–20 Hz energy. In addition, the multi-station stack shows clear moveout of impulsive P-wave arrivals on vertical channels and S-wave arrivals on horizontal channels on seven stations nearest the source location (Figures 1a and 6a; all components shown in Figure S6 in Supporting Information S1). The amplitude of the coda phase decays to noise levels within roughly 10 s of the P arrivals on three of the nearest stations: SEP, VALT, and SUG.

Shallow bursts occur throughout most of 2023 (Figure 4c), during the 2022 swarm from January to March 2022 (Figure 4b), and to a lesser extent the 2016 swarm from March to June 2016. Do shallow burst swarms occur only during these select time periods or are they ubiquitous throughout the entire study period? The compact source region and consistent temporal clustering of events within burst-swarms (Figures 5a and 5b) make it possible for a density-based clustering algorithm to identify individual shallow seismicity bursts. We apply ST- DBSCAN (Birant & Kut, 2007; Cakmak et al., 2021; Ester et al., 1996) on all earthquakes between 2008 and 2024 to automatically detect groups of shallow earthquakes whose locations (X, Y, and depth) and origin times cluster together. ST-DBSCAN is a variant of DBSCAN (Ester et al., 1996) that is designed to accommodate both space

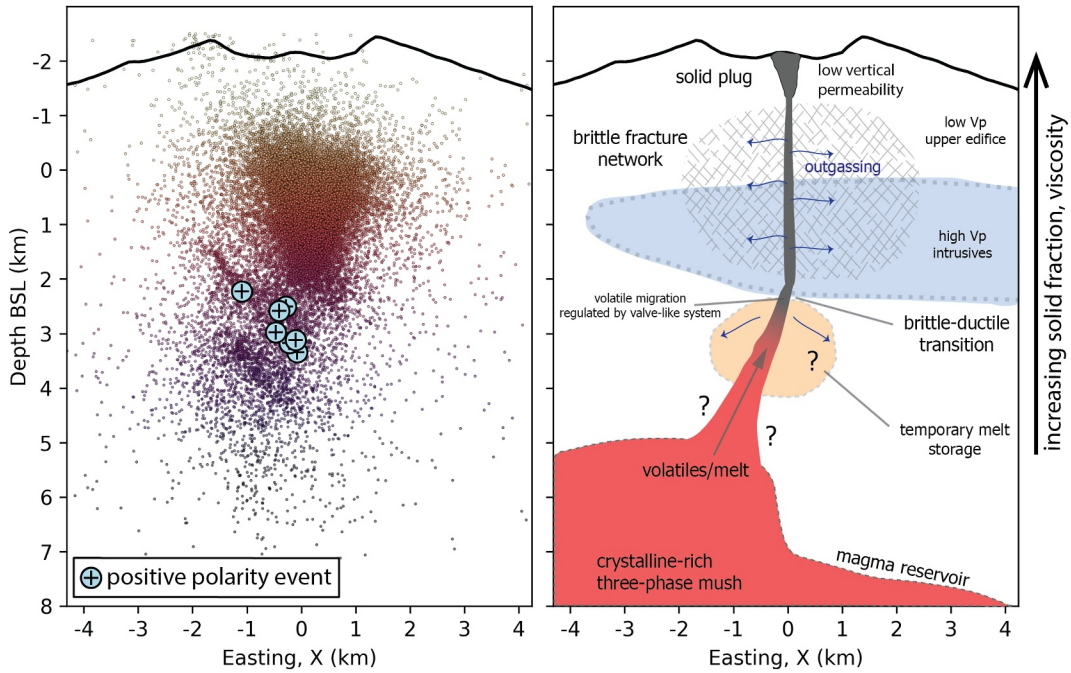

Figure 8. Interpretation of seismogenic features at Mount St. Helens. (a) All earthquake locations along depth, including the locations of 7 events with at least 15 positive and no negative first motion polarities (see Section 3.5 and Figures S11 and S15 in Supporting Information S1). (b) Physical features affecting earthquakes. The magma reservoir and high *Vp* intrusives are traced from the *Vp* images of Kiser et al. (2018). The temporary melt storage zone is loosely based off the shallow magma storage zone from Lees (1992) and Waite and Moran (2009).

and time dimensions. Clusters of data points are formed if the Euclidean distances of constituent points are within a user-defined space and time epsilon and minimum size thresholds relative to each other (Birant & Kut, 2007; Cakmak et al., 2021). We apply spatial and temporal epsilon values of 1 km and 5 hr respectively and require that each cluster include at least 15 events. Lastly, we consider all ST- DBSCAN-identified clusters with a mean location depth shallower than 2 km BSL as shallow burst swarms.

We identify a total of 336 individual shallow seismicity bursts between 2008 and 2024 (Figure 7a). The labels assigned to individual bursts make it convenient to observe statistical patterns including the duration (Figure 7b) and recurrence interval between bursts (Figure 7c). Shallow seismicity bursts occur infrequently between 2008 and 2009, and 2013 and 2015 (Figure 7a). They occur frequently during seismic unrest between 2016 to early 2019 and late 2021 to 2024. All events within shallow seismicity bursts occur within a 1.5 km radius of the dacite domes (Figures 1a, 7f, and 7g), between depths of −1 to 2.5 km BSL (Figures 7g and 7h). The depth distribution of all shallow burst events is densest at approximately 0.25 km BSL. Similarly, with all detected earthquakes in our catalog, events in shallow bursts do not preferentially occur during any season of the year (Figure 7d), or time of day (Figure 7e).

3.5. Source Mechanisms

Our attempts to constrain moment tensor and double-couple solutions are unsuccessful (Figures S9 and S10 in Supporting Information S1). We examine 31 of the most well-recorded events in the PNSN catalog, each of which has at least 15 analyst-picked first-motion polarities. Despite reasonable focal sphere coverage, the resulting moment tensor and double-couple solutions are poorly constrained and contain several misfit polarities (Figures S9 and S10 in Supporting Information S1). This could be due, in part, to difficulties in accurately constraining take-off angles within a complex velocity structure. However, from these 31 events, we find seven events between 2019 and 2022 located within the edifice between 2 and 3.5 km BSL that feature 15 or more positive and no negative first-motion polarities (Figure 8a, Figure S11 in Supporting Information S1). These events feature impulsive P-wave arrivals, show high-frequency energy on borehole stations, and do not correlate with changes in shallow seismicity rates.

4. Discussion

4.1. Volatile Flux as a Driver of VT Seismicity

The driving mechanisms of VT earthquakes are debated and likely specific to the volcanic environment of interest. At Mount St. Helens, we propose that VT seismicity is driven by volatile flux from the shallow magmatic system based on its repetitive swarm-like nature and proximity to the conduit. Although regional-scale tectonic earthquakes occur along the Saint Helens Seismic Zone (SHZ) (Figure S1a in Supporting Information S1) we do not find evidence that tectonic earthquakes on the SHZ are related to seismicity near the Mount St. Helens volcanic edifice (Lehto et al., 2013; Musumeci et al., 2002; Qamar et al., 1981; Weaver et al., 1983).

In this section, we propose that VT seismicity at Mount St. Helens is generated by brittle deformation resulting from increases in fluid pressures on preexisting crack networks within the conduit and the surrounding bedrock (Benson et al., 2008; Goto, 1999; Hill, 1977; Roman & Cashman, 2006; Scholz, 2019; Tuffen et al., 2008). This increase in fluid pressure likely occurs due to volatile flux from the deeper portions of the shallow magma system (Edmonds et al., 2019; Edmonds & Woods, 2018). These volatiles could originate from deeper, aseismic magma injection or from second boiling—the continued release of volatiles during crystallization of magma as it cools post-emplacement (e.g., Roman & Cashman, 2018; Wech et al., 2020). Both processes can increase volatile saturation and have been shown to drive repeating, non-eruptive seismicity in other volcanic environments (Cannata et al., 2013; Wech et al., 2020). Systematic analysis of the long-period seismic records at Mount St. Helens from 2008 to 2024 could help decipher the origin of these volatiles and better constrain their timing and depth.

VT earthquakes at Mount St. Helens have been previously proposed to be associated with shear faulting induced by pressurization within the magmatic conduit and reservoir (Barker & Malone, 1991; Lehto et al., 2010, 2013; Moran, 1994, 2008; Musumeci et al., 2000, 2002; Roman & Cashman, 2006). However, VT earthquakes can encompass a diverse range of source types with varying degrees of double-couple, isotropic, and dipole components (Foulger & Julian, 2015; Hrubcová et al., 2021; Julian et al., 1998; Mildon et al., 2016; Templeton, 2006). Moreover, we find seven earthquakes with all positive first-motion polarities across the focal sphere, suggest that some earthquakes at Mount St. Helens can contain isotropic components (Figures S11 and S15 in Supporting Information S1) (Aki, 1984; Foulger & Julian, 2015).

Spatial and temporal patterns of VT occurrence are also consistent with VTs being driven by volatile flux. Shallow seismicity is much more abundant than deep seismicity between 2008 and 2024 and it is persistent throughout the entire study period. Deep seismicity does not become common until 2016, when it occurs in recurring, semi-periodic swarms that last for several months. Event-rate changes within swarms could signal periods of elevated volatile flux over several weeks to months-long timescales. Shallow seismicity can occur with or without deep seismicity, whereas deep seismicity rarely occurs without concurrent shallow seismicity. If seismicity at all depths is driven by gas flux that originates from the upper-crustal reservoir, it appears to traverse several kilometers of conduit, often without triggering seismicity until it reaches shallow depths. Moreover, this spatial distribution of VTs indicate that the shallow edifice is more prone to brittle deformation than the deep edifice.

We suggest that these macroscopic observations can be explained by (a) a brittle-ductile transition (Fournier, 2007; White & McCausland, 2019) at about 2 km BSL, and (b) reduced vertical permeability toward shallow depth (Figure 8). The proposed brittle-ductile transition at 2 km BSL is roughly consistent with the 80th percentile threshold of focal depths (1.8 km BSL) suggested by Smith and Bruhn (1984). To accommodate these rheological and permeability changes, we consider along-depth changes in the bulk solid fraction of resident magma in the conduit (Figure 8). Upon ascent, magma decompresses and crystallizes as it exsolves volatiles (K. Cashman & Blundy, 2000). In turn, increases in solid fraction within highly crystalline, silicic magma produce substantial changes in viscosity and permeability (Cassidy et al., 2018; Kozono & Koyaguchi, 2012; Schneider et al., 2012; Wong et al., 2017). Small increases in solid fraction can cause increases in magmatic viscosity by several orders of magnitude and affect brittleness of the shallow edifice (K. V. Cashman et al., 2017). Moreover, the resulting loss of volatiles and collapse of pore spaces triggers reduction of porosity, which can decrease permeability by several orders of magnitude in the upper conduit (Heap et al., 2016; Rust & Cashman, 2004; Wong & Segall, 2020). Thus, brittle deformation is favored in shallow depths owing to higher solid volume fraction and

reduced vertical permeability. The resulting mechanical and permeability structures remain in place and serve as the initial conditions that produce VT seismicity thereafter.

Previous imaging of the Mount St. Helens magmatic systems provides some insight into the conduit structure and spatial patterns of VTs. Above 2 km BSL, the shallow seismogenic volume partially overlaps with a tomographically imaged high *Vp* anomaly, which is interpreted as a laterally extensive region of solidified granitic plutons (Figure 8b) (Kiser, 2018; Waite & Moran, 2009). In addition, the base of the seismogenic volume and proposed brittle-ductile transition at 2 km BSL overlaps with a low *Vp* zone previously interpreted as a shallow magma storage region between 2 and 4 km BSL (De Siena et al., 2014; Lees, 1992; Waite & Moran, 2009). This feature, however, is not visible in more recent *Vp* models that use data recorded by the iMUSH experiment between 2014 and 2016 (Kiser et al., 2018; Ulberg et al., 2020). Both Kiser et al. (2018) and Ulberg et al. (2020) suggest that this may have been a temporary feature during and prior to the 2004 to 2008 eruption. At these depths, melt bodies may be unstable and transient (K. V. Cashman et al., 2017). Although the persistence of a shallow magma storage region after the 2004–2008 eruption is unclear, this region may still accumulate transient batches of melt and gases from the upper-crustal reservoir below 5–6 km BSL as it repressurizes (M. Battaglia et al., 2018). Here, melt could be inhibited from migrating upwards due to the lower permeability of the overlying solidified magma. The movement of exsolved volatiles may then be regulated by a valve-like mechanism in the conduit at 2 km BSL, which may either permit it to migrate upwards through the conduit into the shallow fracture network or force it into the surrounding wallrock. Alternatively, upwelling volatiles may concentrate within zones of focused tensile stresses due stiffness contrasts between the melt-rich zone and high-*Vp* intrusive body at 2 km BSL (e.g., Gudmundsson & Brenner, 2004; Kiser et al., 2018).

We infer that VT hypocenters occur within the conduit and surrounding wallrock. Additionally, they trend toward the WSW direction with increasing depth. Deep earthquake hypocenters are less spatially clustered than shallow earthquakes, possibly owing to their larger uncertainties (Figure 3, Figure S8 in Supporting Information S1). Conduit geometry between 2 and 6 km BSL is only loosely constrained as its small aperture makes it difficult to image through tomographic methods. It is unclear if the WSW offset of deep seismicity reflects the geometry of the conduit between 2 and 6 km BSL. However, southwest offset of the lower extent of deep seismicity is consistent with the top of the upper-crustal magmatic reservoir in tomographic images from the iMUSH experiment (Kiser et al., 2018; Ulberg et al., 2020). In addition, the WSW trend of deep hypocenters, given uncertainties, is roughly consistent with the location of a modeled pressurized cylinder proposed by Moran (1994) to explain focal mechanism P-T axis orientations of earthquakes at similar depths from 1987 to 1992.

4.2. Temporal Trends

Shallow background-level seismic activity between 2008 and 2014 can be explained by steady or residual outgassing into the shallow brittle volume and near-magmastatic conditions at the end of the eruption (Anderson & Segall, 2013; Mastin, 2008, 2009; Moran et al., 2011; Segall, 2013; Wong et al., 2017; Wong & Segall, 2019, 2020; Zhang et al., 2022). M. Battaglia et al. (2018) and Makus et al. (2024) interpret magmatic recharge of the upper-crustal reservoir between 2014 and 2016 from observations of mass addition and reduced *Vp* values, respectively. These two observations could indicate the onset timing of precursory recharge leading to seismic unrest, which we observe, beginning in 2016. Episodic deep seismicity swarms between 2016 and 2024 bear some resemblance to deep seismicity swarms between 1987 and 2002 and could similarly be explained by repressurization of exsolved gases from the upper-crustal reservoir that are sealed within the plumbing system by the shallow impermeable dacite plug (Barker and Malone, 1992; Moran, 1994; Moran et al., 2008; Musumeci et al., 2002; Weaver et al., 1983; Zhang et al., 2022). High seismicity rates between 2022 and 2023 may also be explained by repressurization in addition to improved detection thresholds permitted by the installation of four permanent broadband seismometers within 5 km of the edifice between 2018 and 2022 (CC.LOO, CC.REM, CC.USFR and CC.HOA; Figures 1a and 2a, Figure S1 in Supporting Information S1). Deep and shallow seismicity rates within swarms are concurrent within several-month- long timescales but are burst-like and complex within shorter timescales (Zhang et al., 2022). During the initiation of swarms, shallow seismicity rates increase either before or at the same time as deep event rates (Figure 4). Additionally, maximum daily shallow seismicity rates are achieved several weeks to several months before maximum deep earthquake daily rates. These patterns could be explained by a combination of (a) temporary increases in vertical permeability by the formation of volatile flow channels during increased volatile output (Degruyter et al., 2019; Parmigiani et al., 2016, 2017) and (b) the brittle-ductile transition at 2 km BSL (Fournier, 2007; White & McCausland, 2019). Channelized flow pathways may be

able to support volatile flux from the magma reservoir to shallow depths without triggering upward migrating seismicity. In addition, brittle deformation within the conduit beneath 2 km BSL may be inhibited by lower viscosities, however downward-migrating seismicity clusters during peak swarm activity rates indicate that this rheological transition can temporarily migrate to greater depths with high enough strain rates (Cordonnier et al., 2012; Fournier, 2007). Similar rheological transitions are additionally used to explain the lack of pre-eruption seismicity deeper than 0 km BSL (Dzurisin, 2018).

None of the swarms we observe between 2016 and 2024 are associated with detectable ground motion signals recorded by local GNSS stations (Figures S1 and S6 in Supporting Information S1), tiltmeters, or strainmeters. However, deformation consistent with inflation is recorded at local GNSS stations between 2008 and 2012 (Dzurisin et al., 2015; Makus et al., 2024; Palano et al., 2012; Poland et al., 2017). Post-eruptive inflation is ambiguous and could be explained by viscoelastic relaxation with or without contributions from magmatic recharge (M. Battaglia et al., 2018; Segall, 2016, 2019). Deep earthquake swarms in 1989–1992 and 1997 to 1999 coincided with explosive tephra emissions (Mastin, 1994; Moran, 1994) and elevated CO2 levels (Gerlach et al., 2008) respectively. However, there are no detectable outgassing events of CO2, H2S, or SO2 between February 2008 and 2024 (USGS, 2023). The lack of observed H2S and SO2 emissions may be explained by scrubbing interactions with liquid water (Gerlach et al., 2008), but no anomalies that reflect increased outgassing of these chemical species have been detected in measurements from nearby hydrothermal springs (Bedrosian et al., 2007; Bergfeld et al., 2017; Symonds et al., 2001). Based on the absence of eruptive activity, recorded ground deformation consistent with inflation, and gas emissions at Mount St. Helens since January 2008 (Dzurisin, 2018; Dzurisin et al., 2015), we suggest that the "failed eruptions" model proposed by Moran et al. (2011) does not apply to the seismicity swarms we observe in the 2008 to 2024 study period. Thus, the ascent of large volumes of magma through the conduit does not explain the seismicity patterns we observe.

4.3. Shallow Bursts and Repeating Earthquakes

Shallow burst-like VT swarms (Figures 4c, 6, 7) are a curious new discovery revealed by the matched-filter detection and location workflow. Their compact source region, semi-regular periodicity, and waveform similarity may evoke comparison to drumbeat earthquakes recorded during the 2004 to 2008 eruption (Harrington & Brodsky, 2007; Iverson et al., 2006; Matoza & Chouet, 2010; Matoza et al., 2015; Moran et al., 2008; Thelen et al., 2008, 2011; Waite, 2008). However, individual events within shallow seismicity bursts are distinct from drumbeat earthquakes mainly for their lack of dominant long-period energy, which indicates a different source type. Additionally, they are found during non-eruptive earthquake swarms and are roughly 2 km deeper than drumbeat earthquakes. In addition, the lack of long-lived harmonic coda indicates that they do not trigger observable fluid resonance in the conduit (Chouet & Matoza, 2013; Glasgow et al., 2018). In comparison to repeating earthquakes on tectonic structures (e.g., central San Andreas Fault, USA (Nadeau & McEvilly, 2004)), shallow bursts at Mount St. Helens do not repeat over several year-long timescales but similarly occur in pulse-like swarms albeit over much shorter timescales.

Shallow burst-like activity rates are loosely concurrent with deepening swarms (Figures 4 and 7a), indicating a response of the shallow seismogenic volume to gas or fluid input from greater depths. Near-repeating waveforms with 2–20 Hz frequency energy content and consistent locations at −0.5 to 1 km BSL indicate repetitive fracturing within or adjacent to the shallow conduit beneath the dacite domes. In addition, semi-regular time intervals between bursts may reflect quiescent accumulation and valve-like release of fluid or gas overpressure from the conduit into a brittle fracture network (Farge et al., 2021). At Mount St. Helens, a valve at 2 km BSL within the edifice may represent a transient increase in permeability by hydrofracturing or capillary fracturing processes that are characteristic of high-crystallinity magmas (Degruyter et al., 2019; Farge et al., 2021; Oppenheimer et al., 2015; Parmigiani et al., 2016, 2017).

Shallow burst-like events persistently repeat within roughly one month of their respective origin times. Their P- and S-wave arrivals in early to mid 2023 are remarkably similar across this 5-month period (Figure 5c, Figure S7 in Supporting Information S1). By contrast, the steady increase and decay of inter-event cross-correlations leading up to a reference event in Figure 6b can be explained by changes in the coda waveform character (Figure S7 in Supporting Information S1). Hypocenters of individual events within a shallow burst can vary by 1–2 km (Figure 5a). Further refinement of location solutions may be required to verify whether their locations vary by this much or if they collapse into a smaller source volume. S-wave detections, of low signal to noise, that

contain segments of shifted or altered coda wave trains could degrade the cross-correlation measurements, leading to increased hypocenter uncertainty. It is unclear if the progressive change in coda wave character can be explained by changes in location that are not resolved, or due to changes within the scattering medium. However, the consistency of inter-event body-wave cross-correlation values indicates that most events in this time share similar source mechanisms and locations. Well-recorded shallow burst events with mutually similar body waves and changing coda phases may provide an opportunity to image temporal velocity changes near the shallow edifice and flanks (Hotovec-Ellis et al., 2014, 2015; Kanu et al., 2013; Snieder, 2006).

4.4. Environmental Sensitivity

Changes in seismicity rates in response to external factors are well documented in volcanic environments (Brodsky & Van Der Elst, 2014; Hill et al., 1993; Neuberg, 2000). Stress field alterations due to steep thermal gradients between hot solidified magma and rock containing cool meteoric water have been proposed as a mechanism for driving fracturing potential swarm-like seismicity (e.g., Warren & Latham, 1970). However, the role of meteoric fluid in generating VT seismicity at Mount St. Helens is unclear. There are no known instances of seismicity rate changes during non-eruptive periods (i.e., when the vent is shut) in response to large rainfall events. Infiltration times longer than one seasonal cycle are possible; however, electric self-potential measurements made near the edifice indicate that fluid and circulation in the hydrothermal system above roughly 2 km of the surface is fed by magmatic exsolution (Bedrosian et al., 2007). Moreover, at Mount St. Helens, there are few known geologic structures that serve to transmit meteoric fluid deep into the crust (e.g., Lassen Volcano, Long Valley Caldera; Janik & McLaren, 2010; Montgomery-Brown et al., 2019).

Correlations between annual peak seismicity rates and hydrologic well data have been identified at Mount St. Helens and other Cascade Range volcanoes between 1984 and 2004 (Christiansen et al., 2005; Saar & Manga, 2003). The time-of-year frequency histogram of Figure 7d shows a slight increase in event count during the late summer months, when infiltration of snowpack melt is expected to reach its annual maximum flux (Christiansen et al., 2005). However, declustering is necessary to prevent bias due to overrepresentation of seismicity rates from anomalously large swarms. One may also need to explain why there is an additional peak in the January to March months, when snowpack is expected to accumulate. The hypothesis testing required to verify these apparent seasonal correlations are out of scope for this study. Lastly, we do not find any evidence for seismicity rate changes immediately after phase arrivals from global teleseisms of M7 or greater, or regional earthquakes of M3 or greater. Tidal modulation, particularly for periodic shallow seismicity bursts, may be worth consideration. However, most shallow bursts recur within 1–2 days of each other (Figure 7e). If tidal stresses were a primary triggering mechanism, we might expect them to recur within diurnal or semidiurnal periods (Thomas et al., 2009, Scholz, 2019; Wang et al., 2022).

4.5. Implications for Future Eruptive Potential

Increased seismic activity eight years after the end of the 2004 to 2008 eruption of Mount St. Helens indicates increased levels of volatile flux in response to recharge or second boiling within the upper-crustal reservoir, which will eventually lead to the next eruption given sufficient time. Within the past 1,500 years, Mount St. Helens has experienced four 60 to 100 years-long eruptive periods, each consisting of several dome-building eruptions within decades of each other (Evarts et al., 1987; Hoblitt et al., 1980). Despite the apparent increases in subvolcanic activity inferred by seismicity rates, our observations should not be used to forecast the next eruption. Neither the 1980 to 1986 nor 2004 to 2008 dome-building eruptions featured precursory deep seismicity (Dzurisin, 2018; Roman & Cashman, 2018). Moreover, pre-eruptive seismicity is usually shallow and occurs at rates of hundreds of earthquakes per hour--much higher than we observe in our data set (Moran, 1994; Moran et al., 2008; Roman & Cashman, 2018). Further investigations of non-eruptive seismicity, particularly their connection to observations from other disciplines, could be useful to better understand the physical processes that govern eruption cycles.

5. Conclusion

We derive a high-resolution earthquake catalog between 2008 and 2024 to better understand non-eruptive volcanic seismicity at Mount St. Helens. We observe widespread volcano-tectonic VT seismicity in proximity to the conduit between −2 and 7.5 km BSL. Shallow seismicity beneath the volcano's recently emplaced dacite domes within −0.5 to 2 km BSL is persistent from 2008 to 2024, indicating that the shallow edifice is consistently brittle.

Both shallow and deep seismicity rates increase dramatically within semi-periodic earthquake swarms beginning in 2016, indicating increased volatile flux due to recharge or crystallization in the upper-crustal reservoir. Within swarms, peak shallow seismicity rates occur before peak deep seismicity rates. The long-term spatial and temporal seismicity patterns can be explained by a brittle-ductile transition at 2 km BSL and a decrease in vertical permeability within conduit magma toward the shallower edifice—both of which can be attributed to the upward solidification of magma within the conduit. The shallow edifice hosts semi-periodic shallow seismicity bursts that consist of low amplitude repeating earthquakes. Shallow seismicity bursts become frequent beginning in 2016 and tend to occur in temporal proximity to deep earthquake swarms, indicating a valve-like response to gas input from greater depths. Seismicity rates do not appear to change according to seasons of the year nor in response to phase arrivals from large earthquakes at teleseismic or regional distances. Considering these observations, we suggest that non-eruptive VT seismicity at Mount St. Helens is modulated by varying amounts of volatile flux from the upper crustal magma reservoir. Volatiles then interact with structural variations within the conduit that are the result of increasing solid fraction and decreased permeability toward shallow depths.

Conflict of Interest

The authors declare no conflicts of interest relevant to this study.

Data Availability Statement

The earthquake catalog from this study is available in Hirao et al. (2025) and its headers are described in Text S6 in Supporting Information S1. Template event data, including their waveforms and phase arrivals, were obtained from the Pacific Northwest Seismic Network (PNSN; University of Washington, 1963).

Acknowledgments

The earthquake catalog used in this study is provided in Data S1, 10.5281/zenodo.17089016. This material is based upon work supported by the U.S. Geological Survey under Grants G22AP00299 and G22AP00300 and by the National Science Foundation under Award 1848302 and Cooperative Agreement # 2225286. Part of this study was completed during the Pathways Internship at the USGS Geological Hazards Science Center. We offer thanks to Alicia Hotovec-Ellis, Robin Matoza, and an anonymous reviewer for helpful reviews that improved quality of this manuscript. In addition, we extend appreciation to Kathy Cashman, Seth Moran, Alex Iezzi, Gaspard Farge, Rachel Abercrombie, Brandon Schmandt, and Han Zhang for thoughtful discussions. Lastly, we thank Daniel Trugman for help with the GrowClust3D algorithm, Anthony Lomax for help with the NonLinLoc package, the University of Oregon Research Advanced Computing Services staff for their support of the high-performance computing cluster "Talapas," and the staff at the Pacific Northwest Seismic for their earthquake catalog. Any use of trade, firm, or product names is for descriptive purposes only and does not imply endorsement by the U.S. Government.

References

Aki, K. (1984). Evidence for magma intrusion during the Mammoth Lakes Earthquakes of May 1980 and implications of the absence of volcanic (harmonic) tremor. *Journal of Geophysical Research*, *89*(B9), 7689–7696. https://doi.org/10.1029/JB089iB09p07689

Anderson, K., Lisowski, M., & Segall, P. (2010). Cyclic ground tilt associated with the 2004–2008 eruption of Mount St. Helens. *Journal of Geophysical Research*, *115*(B11), 2009JB007102. https://doi.org/10.1029/2009JB007102

Anderson, K., & Segall, P. (2011). Physics-based models of ground deformation and extrusion rate at effusively erupting volcanoes. *Journal of Geophysical Research*, *116*(B7), B07204. https://doi.org/10.1029/2010JB007939

Anderson, K., & Segall, P. (2013). Bayesian inversion of data from effusive volcanic eruptions using physics-based models: Application to Mount St. Helens 2004–2008. *Journal of Geophysical Research: Solid Earth*, *118*(5), 2017–2037. https://doi.org/10.1002/jgrb.50169

Bakun, W. H., & Joyner, W. (1984). The ML scale in central California. *Bulletin of the Seismological Society of America*, *74*(5), 1827–1843. https://doi.org/10.1785/BSSA0740051827

Barker, S. E., & Malone, S. D. (1991). Magmatic system geometry at Mount St. Helens modeled from the stress field associated with posteruptive earthquakes. *Journal of Geophysical Research*, *96*(B7), 11883–11894. https://doi.org/10.1029/91JB00430

Battaglia, J., Thurber, C. H., Got, J., Rowe, C. A., & White, R. A. (2004). Precise relocation of earthquakes following the 15 June 1991 eruption of Mount Pinatubo (Philippines). *Journal of Geophysical Research*, *109*(B7), 2003JB002959. https://doi.org/10.1029/2003JB002959

Battaglia, M., Lisowski, M., Dzurisin, D., Poland, M. P., Schilling, S., Diefenbach, A., & Wynn, J. (2018). Mass addition at Mount St. Helens, Washington, inferred from repeated gravity surveys. *Journal of Geophysical Research: Solid Earth*, *123*(2), 1856–1874. https://doi.org/10.1002/2017JB014990

Bedrosian, P. A., Peacock, J. R., Bowles-Martinez, E., Schultz, A., & Hill, G. J. (2018). Crustal inheritance and a top-down control on arc magmatism at Mount St Helens. *Nature Geoscience*, *11*(11), 865–870. https://doi.org/10.1038/s41561-018-0217-2

Bedrosian, P. A., Unsworth, M. J., & Johnston, M. J. S. (2007). Hydrothermal circulation at Mount St. Helens determined by self-potential measurements. *Journal of Volcanology and Geothermal Research*, *160*(1–2), 137–146. https://doi.org/10.1016/j.jvolgeores.2006.09.003

Benson, P. M., Vinciguerra, S., Meredith, P. G., & Young, R. P. (2008). Laboratory simulation of volcano seismicity. *Science*, *322*(5899), 249–252. https://doi.org/10.1126/science.1161927

Bergfeld, D., Evans, W. C., Spicer, K. R., Hunt, A. G., & Kelly, P. J. (2017). Evidence for degassing of fresh magma during the 2004–2008 eruption of Mount St. Helens: Subtle signals from the hydrothermal system. *Journal of Volcanology and Geothermal Research*, *343*, 109–121. https://doi.org/10.1016/j.jvolgeores.2017.06.020

Beyreuther, M., Barsch, R., Krischer, L., Megies, T., Behr, Y., & Wassermann, J. (2010). ObsPy: A Python toolbox for seismology. *Seismological Research Letters*, *81*(3), 530–533. https://doi.org/10.1785/gssrl.81.3.530

Birant, D., & Kut, A. (2007). ST-DBSCAN: An algorithm for clustering spatial– temporal data. *Data & Knowledge Engineering*, *60*(1), 208–221. https://doi.org/10.1016/j.datak.2006.01.013

Brodsky, E. E., & Van Der Elst, N. J. (2014). The uses of dynamic earthquake triggering. *Annual Review of Earth and Planetary Sciences*, *42*(1), 317–339. https://doi.org/10.1146/annurev-earth-060313-054648

Burjánek, J., Edwards, B., & Fäh, D. (2014). Empirical evidence of local seismic effects at sites with pronounced topography: A systematic approach. *Geophysical Journal International*, *197*(1), 608–619. https://doi.org/10.1093/gji/ggu014

Cakmak, E., Plank, M., Calovi, D. S., Jordan, A., & Keim, D. (2021). Spatio-temporal clustering benchmark for collective animal behavior. *Proceedings of the 1st ACM SIGSPATIAL International Workshop on Animal Movement Ecology and Human Mobility*, 5–8. https://doi.org/10.1145/3486637.3489487

Cannata, A., Alparone, S., & Ursino, A. (2013). Repeating volcano-tectonic earthquakes at mt. Etna volcano (Sicily, Italy) during 1999–2009. *Gondwana Research*, *24*(3–4), 1223–1236. https://doi.org/10.1016/j.gr.2013.02.012

Cascades Volcano Observatory. (2023). *Uptick in earthquake activity remains within background levels*. U.S. Geological Survey. Retrieved from https://www.usgs.gov/observatories/cvo/news/uptick-earthquake-activity-mount-st-helens-remains-within-background-level

Cashman, K., & Blundy, J. (2000). Degassing and crystallization of ascending andesite and dacite. *Philosophical Transactions of the Royal Society of London, Series A: Mathematical, Physical and Engineering Sciences*, *358*(1770), 1487–1513. https://doi.org/10.1098/rsta.2000.0600

Cashman, K. V., & McConnell, S. M. (2005). Multiple levels of magma storage during the 1980 summer eruptions of Mount St. Helens, WA. *Bulletin of Volcanology*, *68*(1), 57–75. https://doi.org/10.1007/s00445-005-0422-x

Cashman, K. V., Sparks, R. S. J., & Blundy, J. D. (2017). Vertically extensive and unstable magmatic systems: A unified view of igneous processes. *Science*, *355*(6331), eaag3055. https://doi.org/10.1126/science.aag3055

Cashman, K. V., Thornber, C. R., & Pallister, J. S. (2008). From dome to dust: Shallow crystallization and fragmentation of conduit magma during the 2004– 2006 dome extrusion of Mount St. Helens. https://doi.org/10.3133/pp175019

Cassidy, M., Manga, M., Cashman, K., & Bachmann, O. (2018). Controls on explosive-effusive volcanic eruption styles. *Nature Communications*, *9*(1), 2839. https://doi.org/10.1038/s41467-018-05293-3

Chouet, B. A. (1996). Long-period volcano seismicity: Its source and use in eruption forecasting. *Nature*, *380*(6572), 309–316. https://doi.org/10.1038/380309a0

Chouet, B. A., & Matoza, R. S. (2013). A multi-decadal view of seismic methods for detecting precursors of magma movement and eruption. *Journal of Volcanology and Geothermal Research*, *252*, 108–175. https://doi.org/10.1016/j.jvolgeores.2012.11.013

Christiansen, L., Hurwitz, S., Saar, M., Ingebritsen, S., & Hsieh, P. (2005). Seasonal seismicity at western United States volcanic centers. *Earth and Planetary Science Letters*, *240*(2), 307–321. https://doi.org/10.1016/j.epsl.2005.09.012

Cordonnier, B., Caricchi, L., Pistone, M., Castro, J., Hess, K.-U., Gottschaller, S., et al. (2012). The viscous-brittle transition of crystal-bearing silicic melt: Direct observation of magma rupture and healing. *Geology*, *40*(7), 611–614. https://doi.org/10.1130/G3914.1

Decker, R., & Decker, B. (1981). The eruptions of Mount St. Helens. *Scientific American*, *244*(3), 68–80. https://doi.org/10.1038/scientificamerican0381-68

Degruyter, W., Parmigiani, A., Huber, C., & Bachmann, O. (2019). How do volatiles escape their shallow magmatic hearth? *Philosophical Transactions of the Royal Society A: Mathematical, Physical and Engineering Sciences*, *377*(2139), 20180017. https://doi.org/10.1098/rsta.2018.0017

Denlinger, R. P., & Moran, S. C. (2014). Volcanic tremor masks its seismogenic source: Results from a study of noneruptive tremor recorded at Mount St. Helens, Washington. *Journal of Geophysical Research: Solid Earth*, *119*(3), 2230–2251. https://doi.org/10.1002/2013JB010698

De Siena, L., Thomas, C., Waite, G. P., Moran, S. C., & Klemme, S. (2014). Attenuation and scattering tomography of the deep plumbing system of Mount St. Helens. *Journal of Geophysical Research: Solid Earth*, *119*(11), 8223–8238. https://doi.org/10.1002/2014JB011372

Dzurisin, D. (2018). Mount St. Helens retrospective: Lessons learned since 1980 and remaining challenges. *Frontiers in Earth Science*, *6*, 142. https://doi.org/10.3389/feart.2018.00142

Dzurisin, D., Moran, S. C., Lisowski, M., Schilling, S. P., Anderson, K. R., & Werner, C. (2015). The 2004–2008 dome-building eruption at Mount St. Helens, Washington: Epilogue. *Bulletin of Volcanology*, *77*(10), 89. https://doi.org/10.1007/s00445-015-0973-4

Dzurisin, D., Vallance, J. W., Gerlach, T. M., Moran, S. C., & Malone, S. D. (2005). Mount St. Helens reawakens. *Eos, Transactions American Geophysical Union*, *86*(3), 25–29. https://doi.org/10.1029/2005EO030001

Eaton, J., & Murata, K. (1960). How volcanoes grow. *Science*, *132*(3432), 925–938. https://doi.org/10.1126/science.132.3432.925

Edmonds, M., Cashman, K. V., Holness, M., & Jackson, M. (2019). Architecture and dynamics of magma reservoirs. *Philosophical Transactions of the Royal Society A: Mathematical, Physical and Engineering Sciences*, *377*(2139), 20180298. https://doi.org/10.1098/rsta.2018.0298

Edmonds, M., & Woods, A. W. (2018). Exsolved volatiles in magma reservoirs. *Journal of Volcanology and Geothermal Research*, *368*, 13–30. https://doi.org/10.1016/j.jvolgeores.2018.10.018

Endo, E. T., Malone, S. D., Noson, L. L., & Weaver, C. S. (1981). Locations, magnitudes, and statistics of the March 20–May 18 earthquake sequence. In P. W. Lipman & D. R. Mullineaux (Eds.), *The 1980 eruptions of Mount St. Helens, Washington* (pp. 93–108). https://doi.org/10.3133/pp1250

Ester, M., Kriegel, H.-P., & Xu, X. (1996). A density-based algorithm for discovering clusters in large spatial databases with noise. *Proceedings of the 2nd International Conference on Knowledge Discovery and Data Mining (KDD-96)*, 226–231. https://doi.org/10.5555/3001460.3001507

Evarts, R. C., Ashley, R. P., & Smith, J. G. (1987). Geology of the Mount St. Helens area: Record of discontinuous volcanic and plutonic activity in the Cascade Arc of southern Washington. *Journal of Geophysical Research*, *92*(B10), 10155–10169. https://doi.org/10.1029/JB092iB10p10155

Farge, G., Jaupart, C., & Shapiro, N. M. (2021). Episodicity and migration of low frequency earthquakes modeled with fast fluid pressure transients in the permeable subduction interface. *Journal of Geophysical Research: Solid Earth*, *126*(9), e2021JB021894. https://doi.org/10.1029/2021JB021894

Fehler, M. (1983). Observations of volcanic tremor at Mount St. Helens volcano. *Journal of Geophysical Research*, *88*(B4), 3476–3484. https://doi.org/10.1029/JB088iB04p03476

Fehler, M., & Chouet, B. (1982). Operation of a digital seismic network on Mount St. Helens volcano and observations of long period seismic events that originate under the volcano. *Geophysical Research Letters*, *9*, 1017–1020. https://doi.org/10.1029/GL009i009p01017

Foulger, G. R., & Julian, B. R. (2015). Non-double-couple earthquakes. In M. Beer, I. A. Kougioumtzoglou, E. Patelli, & I. S.-K. Au (Eds.), *Encyclopedia of earthquake engineering* (pp. 1–31). Springer Berlin Heidelberg. https://doi.org/10.1007/978-3-642-36197-5_290-1

Fournier, R. O. (2007). Hydrothermal systems and volcano geochemistry. In D. Dzurisin (Ed.), *Volcano deformation*. Springer. https://doi.org/10.1007/978-3-540-49302-0_10

Gabrielli, S., Spagnolo, M., & De Siena, L. (2020). Geomorphology and surface geology of Mount St. Helens volcano. *Journal of Maps*, *16*(2), 585–594. https://doi.org/10.1080/17445647.2020.1790048

Garza-Girón, R., Brodsky, E. E., Spica, Z. J., Haney, M. M., & Webley, P. W. (2023). A specific earthquake processing workflow for studying long-lived, explosive volcanic eruptions with application to the 2008 okmok volcano, Alaska, eruption. *Journal of Geophysical Research: Solid Earth*, *128*(5), e2022JB025882. https://doi.org/10.1029/2022JB025882

Gaunt, H. E., Sammonds, P. R., Meredith, P. G., & Chadderton, A. (2016). Effect of temperature on the permeability of lava dome rocks from the 2004–2008 eruption of Mount St. Helens. *Bulletin of Volcanology*, *78*(4), 30. https://doi.org/10.1007/s00445-016-1024-5

Gaunt, H. E., Sammonds, P. R., Meredith, P. G., Smith, R., & Pallister, J. S. (2014). Pathways for degassing during the lava dome eruption of Mount St. Helens 2004–2008. *Geology*, *42*(11), 947–950. https://doi.org/10.1130/G35940.1

Gerlach, T. M., McGee, K. A., & Doukas, M. P. (2008). *Emission rates of CO_2, SO_2, and H_2S, scrubbing, and preeruption excess volatiles at Mount St. Helens, 2004–2005*. U.S. Geological Survey Professional Paper 1750-26. https://doi.org/10.3133/pp175026

Glasgow, M. E., Schmandt, B., & Hansen, S. M. (2018). Upper crustal low-frequency seismicity at Mount St. Helens detected with a dense geophone array. *Journal of Volcanology and Geothermal Research*, *358*, 329–341. https://doi.org/10.1016/j.jvolgeores.2018.06.006

Gleeson, M. (2020). Mount St helens 40 years on. *Nature Reviews Earth & 959 Environment*, *1*(6), 283. https://doi.org/10.1038/s43017-020-0059-5

Goto, A. (1999). A new model for volcanic earthquake at Unzen volcano: Melt rupture model. *Geophysical Research Letters*, *26*(16), 2541–2544. https://doi.org/10.1029/1999GL900569

Gudmundsson, A., & Brenner, S. L. (2004). How mechanical layering affects local stresses, unrests, and eruptions of volcanoes. *Geophysical Research Letters*, *31*(16), 2004GL020083. https://doi.org/10.1029/2004GL020083

Han, J., Vidale, J. E., Houston, H., Schmidt, D. A., & Creager, K. C. (2018). Deep long-period earthquakes beneath Mount St. Helens: Their relationship to tidal stress, episodic tremor and slip, and regular earthquakes. *Geophysical Research Letters*, *45*(5), 2241–2247. https://doi.org/10.1002/2018GL077063

Hansen, S. M., & Schmandt, B. (2015). Automated detection and location of microseismicity at Mount St. Helens with a large-N geophone array. *Geophysical Research Letters*, *42*(18), 7390–7397. https://doi.org/10.1002/2015GL064848

Hardebeck, J. L., & Shearer, P. M. (2003). Using S/P amplitude ratios to constrain the focal mechanisms of small earthquakes. *Bulletin of the Seismological Society of America*, *93*(6), 2434–2444. https://doi.org/10.1785/0120020236

Harrington, R. M., & Brodsky, E. E. (2007). Volcanic hybrid earthquakes that are brittle-failure events. *Geophysical Research Letters*, *34*(6), 2006GL028714. https://doi.org/10.1029/2006GL028714

Heap, M. J., Russell, J. K., & Kennedy, L. A. (2016). Mechanical behaviour of dacite from Mount St. Helens (USA): A link between porosity and lava dome extrusion mechanism (dome or spine)? *Journal of Volcanology and Geothermal Research*, *328*, 159–177. https://doi.org/10.1016/j.jvolgeores.2016.10.015

Hill, D. P. (1977). A model for earthquake swarms. *Journal of Geophysical Research*, *82*(8), 1347–1352. https://doi.org/10.1029/JB082i008p01347

Hill, D. P., Reasenberg, P. A., Michael, A., Arabaz, W. J., Beroza, G., Brumbaugh, D., et al. (1993). Seismicity remotely triggered by the magnitude 7.3 landers, California, earthquake. *Science*, *260*(5114), 1617–1623. https://doi.org/10.1126/science.260.5114.1617

Hirao, B., Thomas, A., Shelly, D., Thelen, W., & Journeau, C. (2025). Dataset for: Magmatic volatile flux drives non-eruptive volcano-tectonic seismicity at Mount St. Helens, USA from 2008-2023 [Dataset]. *Journal of Geophysical Research: Solid Earth*. https://doi.org/10.5281/zenodo.17089016

Hoblitt, R. P., Crandell, D. R., & Mullineaux, D. R. (1980). Mount St. Helens eruptive behavior during the past 1,500 yr. *Geology*, *8*(11), 555. https://doi.org/10.1130/0091-7613(1980)8<555:MSHEBD>2.0.CO;2

Hotovec-Ellis, A. J., Gomberg, J., Vidale, J. E., & Creager, K. C. (2014). A continuous record of intereruption velocity change at Mount St. Helens from coda wave interferometry. *Journal of Geophysical Research: Solid Earth*, *119*(3), 2199–2214. https://doi.org/10.1002/2013JB010742

Hotovec-Ellis, A. J., Shelly, D. R., Hill, D. P., Pitt, A. M., Dawson, P. B., & Chouet, B. A. (2018). Deep fluid pathways beneath Mammoth Mountain, California, illuminated by migrating earthquake swarms. *Science Advances*, *4*(8), eaat5258. https://doi.org/10.1126/sciadv.aat5258

Hotovec-Ellis, A. J., Vidale, J. E., Gomberg, J., Thelen, W., & Moran, S. C. (2015). Changes in seismic velocity during the first 14 months of the 2004–2008 eruption of Mount St. Helens, Washington. *Journal of Geophysical Research: Solid Earth*, *120*(9), 6226–6240. https://doi.org/10.1002/2015JB012101

Hrubcová, P., Doubravová, J., & Vavryčuk, V. (2021). Non-double-couple earthquakes in 2017 swarm in Reykjanes Peninsula, SW Iceland: Sensitive indicator of volcano-tectonic movements at slow-spreading rift. *Earth and Planetary Science Letters*, *563*, 116875. https://doi.org/10.1016/j.epsl.2021.116875

Iverson, R. M., Dzurisin, D., Gardner, C. A., Gerlach, T. M., LaHusen, R. G., Lisowski, M., et al. (2006). Dynamics of seismogenic volcanic extrusion at Mount St Helens in 2004–05. *Nature*, *444*(7118), 439–443. https://doi.org/10.1038/nature05322

Janik, C. J., & McLaren, M. K. (2010). Seismicity and fluid geochemistry at Lassen volcanic National Park, California: Evidence for two circulation cells in the hydrothermal system. *Journal of Volcanology and Geothermal Research*, *189*(3–4), 257–277. https://doi.org/10.1016/j.jvolgeores.2009.11.014

Julian, B. R., Miller, A. D., & Foulger, G. R. (1998). Non-double-couple earthquakes 1. Theory. *Reviews of Geophysics*, *36*(4), 525–549. https://doi.org/10.1029/98RG00716

Kanu, C. O., Snieder, R., & O'Connell, D. (2013). Estimation of velocity change using repeating earthquakes with different locations and focal mechanisms. *Journal of Geophysical Research: Solid Earth*, *118*(6), 2905–2914. https://doi.org/10.1002/jgrb.50206

Kiser, E., Levander, A., Schmandt, B., & Hansen, S. (2021). Seismic evidence of Bottom-Up crustal control on volcanism and magma storage near Mount St. Helens. *Geophysical Research Letters*, *48*(5), e2020GL090612. https://doi.org/10.1029/2020GL090612

Kiser, E., Levander, A., Zelt, C., Schmandt, B., & Hansen, S. (2018). Focusing of melt near the top of the Mount St. Helens (USA) magma reservoir and its relationship to major volcanic eruptions. *Geology*, *46*(9), 775–778. https://doi.org/10.1130/G45140.1

Kiser, E., Levander, A., Zelt, C., Schmandt, B., & Hansen, S. (2019). Upper crustal structure and magmatism in Southwest Washington: Vp, Vs, and Vp/Vs results from the iMUSH active-source seismic experiment. *Journal of Geophysical Research: Solid Earth*, *124*(7), 7067–7080. https://doi.org/10.1029/2018JB016203

Kiser, E., Palomeras, I., Levander, A., Zelt, C., Harder, S., Schmandt, B., et al. (2016). Magma reservoirs from the upper crust to the Moho inferred from high-resolution Vp and Vs models beneath Mount St. Helens, Washington State, USA. *Geology*, *44*(6), 411–414. https://doi.org/10.1130/G37591.1

Klein, F. W., Koyanagi, R., Nakata, J., & Tanigawa, W. (1987). The seismicity of Kilaueas's magma System. In R. W. Decker, T. L. Wright, & P. H. Stauffer (Eds.), *Volcanism in Hawaii: USGS professional paper 1350* (pp. 1019–1185).

Köpfli, M., Denolle, M. A., Thelen, W. A., Makus, P., & Malone, S. D. (2024). Examining 22 years of ambient seismic wavefield at Mount St. Helens. *Seismological Research Letters*, *95*(5), 2622–2636. https://doi.org/10.1785/0220240079

Kozono, T., & Koyaguchi, T. (2012). Effects of gas escape and crystallization on the complexity of conduit flow dynamics during lava dome eruptions. *Journal of Geophysical Research*, *117*(B8), 2012JB009343. https://doi.org/10.1029/2012JB00934

Lapins, S. (2022). Python functions to estimate completeness magnitudes and b-values for catalogues of seismicity. *GitHub*. https://github.com/sachalapins/bvalues/blob/main/bvalues.ipynb

Leeman, W. P., & Smith, D. R. (2018). The role of magma mixing, identification of mafic magma inputs, and structure of the underlying magmatic system at Mount St. Helens. *American Mineralogist*, *103*(12), 1925–1944. https://doi.org/10.2138/am-2018-6555

Lees, J. M. (1992). The magma system of Mount St. Helens: Non-linear high-resolution P-wave tomography. *Journal of Volcanology and Geothermal Research*, *53*(1–4), 103–116. https://doi.org/10.1016/0377-0273(92)90077-Q

Lehto, H. L., Roman, D. C., & Moran, S. C. (2010). Temporal changes in stress preceding the 2004–2008 eruption of Mount St. Helens, Washington. *Journal of Volcanology and Geothermal Research*, *198*(1–2), 129–142. https://doi.org/10.1016/j.jvolgeores.2010.08.015

Lehto, H. L., Roman, D. C., & Moran, S. C. (2013). Source mechanisms of persistent shallow earthquakes during eruptive and non-eruptive periods between 1981 and 2011 at Mount St. Helens, Washington. *Journal of Volcanology and Geothermal Research*, *256*, 1–15. https://doi.org/10.1016/j.jvolgeores.2013.02.005

Lipman, P. W., & Mullineaux, D. R. (1981). *The 1980 eruptions of Mount St. Helens*. U.S. Geological Survey Professional Paper 1250.

Lomax, A., Michelini, A., & Curtis, A. (2014). Earthquake location, direct, Global- search methods. In R. Meyers (Ed.), *Encyclopedia of complexity and systems science*. Springer. https://doi.org/10.1007/978-3-642-27737-5_150-2

Lomax, A., Virieux, J., Volant, P., & Berge-Thierry, C. (2000). Probabilistic earthquake location in 3D and layered models. In C. H. Thurber & N. Rabinowitz (Eds.), *Advances in seismic event location* (Vol. 18, pp. 101–134). Springer. https://doi.org/10.1007/978-94-015-9536-0_5

Major, J. J., Scott, W. E., Driedger, C., & Dzurisin, D. (2005). *Mount St. Helens erupts again; activity from September 2004 through March 2005* (pp. 4). U.S. Geological Survey Fact Sheet.

Makus, P., Denolle, M. A., Sens-Schönfelder, C., Köpfli, M., & Tilmann, F. (2024). Analyzing volcanic, tectonic, and environmental influences on the seismic velocity from 25 years of data at Mount St. Helens. *Seismological Research Letters*, *95*(5), 2674–2688. https://doi.org/10.1785/0220240088

Malone, S. D. (2020). Recovering analog-tape seismograms from the 1980 Mount St. Helens pre-eruption period. *Seismological Research Letters*, *91*(3), 1430–1440. https://doi.org/10.1785/0220190327

Malone, S. D., Boyko, C., & Weaver, C. S. (1983). Seismic precursors to the Mount St. Helens eruptions in 1981 and 1982. *Science*, *221*(4618), 1376–1378. https://doi.org/10.1126/science.221.4618.1376

Mastin, L. G. (1994). Explosive tephra emissions at Mount St. Helens, 1989-1991: The violent escape of magmatic gas following storms? *Geological Society of America Bulletin*, *106*(2), 175–185. https://doi.org/10.1130/0016-7606(1994)106<0175:ETEAMS>2.3.CO;2

Mastin, L. G., Lisowski, M., Roeloffs, E., & Beeler, N. (2009). Improved constraints on the estimated size and volatile content of the Mount St. Helens magma system from the 2004–2008 history of dome growth and deformation. *Geophysical Research Letters*, *36*(20), 2009GL039863. https://doi.org/10.1029/2009GL039863

Mastin, L. G., Roeloffs, E., Beeler, N. M., & Quick, J. E. (2008). Constraints on the size, overpressure, and volatile content of the Mount St. Helens magma System from geodetic and dome-growth measurements during the 2004– 2006+ eruption. In D. R. Sherrod, W. E. Scott, & P. H. Stauffer (Eds.), *A volcano rekindled: The renewed eruption of Mount St. Helens, 2004–2006* (pp. 461–492). U.S. Geological Survey. https://doi.org/10.3133/pp175022

Matoza, R. S., & Chouet, B. A. (2010). Subevents of long-period seismicity: Implications for hydrothermal dynamics during the 2004–2008 eruption of Mount St. Helens. *Journal of Geophysical Research*, *115*(B12), 2010JB007839. https://doi.org/10.1029/2010JB007839

Matoza, R. S., Chouet, B. A., Dawson, P. B., Shearer, P. M., Haney, M. M., Waite, G. P., et al. (2015). Source mechanism of small long-period events at Mount St. Helens in July 2005 using template matching, phase-weighted stacking, and full-waveform inversion. *Journal of Geophysical Research: Solid Earth*, *120*(9), 6351–6364. https://doi.org/10.1002/2015JB012279

McNutt, S. R., & Roman, D. C. (2015). Volcanic seismicity. In *The encyclopedia of volcanoes* (pp. 1011–1034). Elsevier. https://doi.org/10.1016/B978-0-12-385938-9.00059-6

Mildon, Z. K., Pugh, D. J., Tarasewicz, J., White, R. S., & Brandsdóttir, B. (2016). Closing crack earthquakes within the Krafla caldera, North Iceland. *Geophysical Journal International*, *207*(2), 1137–1141. https://doi.org/10.1093/gji/ggw325

Minakami, T. (1974). Seismology of volcanoes in Japan. *Developments in Solid Earth Geophysics*, *6*, 1–27. https://doi.org/10.1016/b978-0-444-41141-9.50007-3

Montgomery-Brown, E. K., Shelly, D. R., & Hsieh, P. A. (2019). Snowmelt-triggered earthquake swarms at the margin of long Valley Caldera, California. *Geophysical Research Letters*, *46*(21), 3698–3705. https://doi.org/10.1029/2019GL082254

Moran, S. C. (1994). Seismicity at Mount St. Helens, 1987–1992: Evidence for repressurization of an active magmatic system. *Journal of Geophysical Research*, *99*(B3), 4341–4354. https://doi.org/10.1029/93JB02993

Moran, S. C., Malone, S. D., Qamar, A. I., Thelen, W. A., Wright, A. K., & Caplan-Auerbach, J. (2008). Seismicity associated with renewed dome building at Mount St. Helens, 2004–2005. https://doi.org/10.3133/pp17502

Moran, S. C., Newhall, C., & Roman, D. C. (2011). Failed magmatic eruptions: Late-stage cessation of magma ascent. *Bulletin of Volcanology*, *73*(2), 115–122. https://doi.org/10.1007/s00445-010-0444-x

Moser, T. J. (1991). Shortest path calculation of seismic rays. *Geophysics*, *56*(1), 59–67. https://doi.org/10.1190/1.1442958

Musumeci, C., Malone, S. D., Giampiccolo, E., & Gresta, S. (2000). Stress tensor computations at Mount St. Helens (1995 – 1998). *Annals of Geophysics*, *43*(5), 889–904. https://doi.org/10.4401/ag-3681

Musumeci, C., Gresta, S., & Malone, S. D. (2002). Magma system recharge of Mount St. Helens from precise relative hypocenter location of microearthquakes. *Journal of Geophysical Research*, *107*(B10). https://doi.org/10.1029/2001JB000629

Nadeau, R. M., & McEvilly, T. V. (2004). Periodic pulsing of characteristic microearthquakes on the San Andreas fault. *Science*, *303*(5655), 220–222. https://doi.org/10.1126/science.1090353

NASA Shuttle Radar Topography Mission (SRTM). (2013). Shuttle radar topography mission (SRTM) global. Distributed by OpenTopography. https://doi.org/10.5069/G9445JDF

Neuberg, J. (2000). External modulation of volcanic activity. *Geophysical Journal International*, *142*(1), 232–240. https://doi.org/10.1046/j.1365-246x.2000.00161.x

Neuberg, J., & Pointer, T. (2000). Effects of volcano topography on seismic broad-band waveforms. *Geophysical Journal International*, *143*(1), 239–248. https://doi.org/10.1046/j.1365-246x.2000.00251.x

Nichols, M. L., Malone, S. D., Moran, S. C., Thelen, W. A., & Vidale, J. E. (2011). Deep long-period earthquakes beneath Washington and Oregon volcanoes. *Journal of Volcanology and Geothermal Research*, *200*(3–4), 116–128. https://doi.org/10.1016/j.jvolgeores.2010.12.005

Oppenheimer, J., Rust, A. C., Cashman, K. V., & Sandnes, B. (2015). Gas migration regimes and outgassing in particle-rich suspensions. *Frontiers in Physics*, *3*. https://doi.org/10.3389/fphy.2015.00060

Palano, M., Guarrera, E., & Mattia, M. (2012). GPS ground deformation patterns at Mount St. Helens (Washington, USA) from 2004 to 2010. *Terra Nova*, *24*(2), 148–155. https://doi.org/10.1111/j.1365-3121.2011.01049.x

Pallister, J. S., Cashman, K. V., Hagstrum, J. T., Beeler, N. M., Moran, S. C., & Denlinger, R. P. (2013). Faulting within the Mount St. Helens conduit and implications for volcanic earthquakes. *Geological Society of America Bulletin*, *125*(3–4), 359–376. https://doi.org/10.1130/B30716.1

Pallister, J. S., Hoblitt, R. P., Crandell, D. R., & Mullineaux, D. R. (1992). Mount St. Helens a decade after the 1980 eruptions: Magmatic models, chemical cycles, and a revised hazards assessment. *Bulletin of Volcanology*, *54*(2), 126–146. https://doi.org/10.1007/BF00278003

Pallister, J. S., Thornber, C. R., Cashman, K. V., Clynne, M. A., Lowers, H. A., Mandeville, C. W., et al. (2008). Petrology of the 2004–2006 Mount St. Helens lava dome—Implications for magmatic plumbing and eruption triggering. In D. R. Sherrod, W. E. Scott, & P. H.

Stauffer (Eds.), *A volcano rekindled: The renewed eruption of Mount St. Helens, 2004–2006* (pp. 647–702). U.S. Geological Survey. https://doi.org/10.3133/pp175030

Parmigiani, A., Degruyter, W., Leclaire, S., Huber, C., & Bachmann, O. (2017). The mechanics of shallow magma reservoir outgassing. *Geochemistry, Geophysics, Geosystems*, *18*(8), 2887–2905. https://doi.org/10.1002/2017GC006912

Parmigiani, A., Faroughi, S., Huber, C., Bachmann, O., & Su, Y. (2016). Bubble accumulation and its role in the evolution of magma reservoirs in the upper crust. *Nature*, *532*(7600), 492–495. https://doi.org/10.1038/nature17401

Poland, M. P., Lisowski, M., Dzurisin, D., Kramer, R., McLay, M., & Pauk, B. (2017). Volcano geodesy in the Cascade arc, USA. *Bulletin of Volcanology*, *79*(8), 59. https://doi.org/10.1007/s00445-017-1140-x

Power, J. A., Lahr, J. C., Page, R. A., Chouet, B. A., Stephens, C. D., Harlow, D. H., et al. (1994). Seismic evolution of the 1989–1990 eruption sequence of Redoubt Volcano, Alaska. *Journal of Volcanology and Geothermal Research*, *62*(1–4), 69–94. https://doi.org/10.1016/0377-0273(94)90029-9

Pugh, D. J., & White, R. S. (2018). MTfit: A bayesian approach to seismic moment tensor inversion. *Seismological Research Letters*, *89*(4), 1507–1513. https://doi.org/10.1785/0220170273

Qamar, A., Rathbun, A., Ludwin, R., Noson, L. L., Crosson, R. S., & Malone, S. D. (1981). Earthquake hypocenters in Washington and northern Oregon-198. *Washington State Department of Natural Resources, Division of Geology and Earth Resources*. https://www.dnr.wa.gov/publications/ger_ic83_eq_hypocenters_western_wa_1981.pdf

Ripperger, J., Igel, H., & Wasserman, J. (2003). Seismic wave simulation in the presence of real volcano topography. *Journal of Volcanology and Geothermal Research*, *128*(1–3), 31–44. https://doi.org/10.1016/S0377-0273(03)00245-2

Roman, D. C., & Cashman, K. V. (2006). The origin of volcano-tectonic earthquake swarms. *Geology*, *34*(6), 457. https://doi.org/10.1130/G22269.1

Roman, D. C., & Cashman, K. V. (2018). Top–down precursory volcanic seismicity: Implications for stealth magma ascent and long-term eruption forecasting. *Frontiers in Earth Science*, *6*, 124. https://doi.org/10.3389/feart.2018.00124

Ross, Z. E., Trugman, D. T., Hauksson, E., & Shearer, P. M. (2019). Searching for hidden earthquakes in Southern California. *Science*, *364*(6442), 767–771. https://doi.org/10.1126/science.aaw6888

Rust, A. C., & Cashman, K. V. (2004). Permeability of vesicular silicic magma: Inertial and hysteresis effects. *Earth and Planetary Science Letters*, *228*(1–2), 93–107. https://doi.org/10.1016/j.epsl.2004.09.025

Rutherford, M. J., & Hill, P. M. (1993). Magma ascent rates from amphibole breakdown: An experimental study applied to the 1980–1986 Mount St. Helens eruptions. *Journal of Geophysical Research*, *98*(B11), 19667–19685. https://doi.org/10.1029/93JB01613

Saar, M. O., & Manga, M. (2003). Seismicity induced by seasonal groundwater recharge at mt. Hood, Oregon. *Earth and Planetary Science Letters*, *214*(3–4), 605–618. https://doi.org/10.1016/S0012-821X(03)00418-7

Scandone, R., & Malone, S. D. (1985). Magma supply, magma discharge and readjustment of the feeding system of Mount St. Helens during 1980. *Journal of Volcanology and Geothermal Research*, *23*(3–4), 239–262. https://doi.org/10.1016/0377-0273(85)90036-8

Schneider, A., Rempel, A. W., & Cashman, K. V. (2012). Conduit degassing and thermal controls on eruption styles at Mount St. Helens. *Earth and Planetary Science Letters*, *357–358*, 347–354. https://doi.org/10.1016/j.epsl.2012.09.045

Scholz, C. H. (2019). *The mechanics of earthquakes and faulting* (3rd ed.). Cambridge University Press. https://doi.org/10.1017/9781316681473

Segall, P. (2013). Volcano deformation and eruption forecasting. *Geological Society*, *380*, 85–106. https://doi.org/10.1144/SP380.4

Segall, P. (2016). Repressurization following eruption from a magma chamber with a viscoelastic aureole. *Journal of Geophysical Research: Solid Earth*, *121*(12), 8501–8522. https://doi.org/10.1002/2016JB013597

Segall, P. (2019). Magma chambers: What we can, and cannot, learn from volcano geodesy. *Philosophical Transactions of the Royal Society A: Mathematical, Physical and Engineering Sciences*, *377*(2139), 20180158. https://doi.org/10.1098/rsta.2018.0158

Senobari, N. S., Funning, G. J., Keogh, E., Zhu, Y., Yeh, C. M., Zimmerman, Z., & Mueen, A. (2019). Super-efficient cross-correlation (SEC-C): A fast matched filtering code suitable for desktop computers. *Seismological Research Letters*, *90*(1), 322–334. https://doi.org/10.1785/0220180122

Shelly, D. R., Ellsworth, W. L., & Hill, D. P. (2016). Fluid-faulting evolution in high definition: Connecting fault structure and frequency-magnitude variations during the 2014 Long Valley Caldera, California, earthquake swarm. *Journal of Geophysical Research: Solid Earth*, *121*(3), 1776–1795. https://doi.org/10.1002/2015JB012719

Shelly, D. R., Hill, D. P., Massin, F., Farrell, J., Smith, R. B., & Taira, T. (2013). A fluid-driven earthquake swarm on the margin of the Yellowstone caldera. *Journal of Geophysical Research: Solid Earth*, *118*(9), 4872–4886. https://doi.org/10.1002/jgrb.50362

Sherrod, D. R., Scott, W. E., & Stauffer, P. H. (Eds.) (2008). *A volcano rekindled; the renewed eruption of Mount St. Helens, 2004-2006*. U.S. Geological Survey Professional Paper 1750. Retrieved from https://pubs.usgs.gov/pp/1750/

Smith, D. R., & Leeman, W. P. (1993). The origin of Mount St. Helens andesites. *Journal of Volcanology and Geothermal Research*, *55*(3–4), 271–303. https://doi.org/10.1016/0377-0273(93)90042-P

Smith, R. B., & Bruhn, R. L. (1984). Intraplate extensional tectonics of the Eastern basin-Range: Inferences on structural style from seismic reflection data, regional tectonics, and thermal-mechanical models of brittle-ductile deformation. *Journal of Geophysical Research*, *89*(B7), 5733–5762. https://doi.org/10.1029/JB089iB07p05733

Snieder, R. (2006). The theory of coda wave interferometry. *Pure and Applied Geophysics*, *163*(2–3), 455–473. https://doi.org/10.1007/s00024-005-0026-6

Stanley, W. D., Mooney, W. D., & Fuis, G. S. (1990). Deep crustal structure of the Cascade Range and surrounding regions from seismic refraction and magnetotelluric data. *Journal of Geophysical Research*, *95*(B12), 19419–19438. https://doi.org/10.1029/JB095iB12p19419

Stephens, C. D., Chouet, B. A., Page, R. A., Lahr, J. C., & Power, J. A. (1994). Seismological aspects of the 1989–1990 eruptions at redoubt volcano, Alaska: The SSAM perspective. *Journal of Volcanology and Geothermal Research*, *62*(1–4), 153–182. https://doi.org/10.1016/0377-0273(94)90032-9

Swanson, D. A., Casadevall, T. J., Dzurisin, D., Holcomb, R. T., Newhall, C. G., Malone, S. D., & Weaver, C. S. (1985). Forecasts and predictions of eruptive activity at Mount St. Helens, USA–1975-1984. *Journal of Geodynamics*, *3*(3–4), 397–423. https://doi.org/10.1016/0264-3707(85)90044-4

Symonds, R. B., Gerlach, T. M., & Reed, M. H. (2001). Magmatic gas scrubbing: Implications for volcano monitoring. *Journal of Volcanology and Geothermal Research*, *108*(1–4), 303–341. https://doi.org/10.1016/S0377-0273(00)00292-4

Templeton, D. C. (2006). Non-double-couple earthquakes in the long Valley volcanic Region. *Bulletin of the Seismological Society of America*, *96*(1), 69–79. https://doi.org/10.1785/0120040206

Thelen, W., Malone, S., & West, M. (2011). Multiplets: Their behavior and utility at dacitic and andesitic volcanic centers. *Journal of Geophysical Research*, *116*(B8), B08210. https://doi.org/10.1029/2010JB007924

Thomas, A., Nadeau, R., & Bürgmann, R. (2009). Tremor-tide correlations and near-lithostatic pore pressure on the deep San Andreas fault. *Nature*, *462*(7276), 1048–1051. https://doi.org/10.1038/nature08654

Toomey, D. R., Solomon, S. C., & Purdy, G. M. (1994). Tomographic imaging of the shallow crustal structure of the East Pacific Rise at 9°30′N. *Journal of Geophysical Research*, *99*(B12), 24135–24157. https://doi.org/10.1029/94JB01942

Topinka, L. (2004). *Mount St. Helens, Washington – Summary. The volcanoes of lewis and clark*. U.S. Geological Survey. Retrieved from https://volcanoes.usgs.gov/observatories/cvo/Historical/LewisClark/Info/summary_mount_st_helens.shtml

Trugman, D. T., Chamberlain, C. J., Savvaidis, A., & Lomax, A. (2023). GrowClust3D.jl: A julia package for the relative relocation of earthquake hypocenters using 3D velocity models. *Seismological Research Letters*, *94*(1), 443–456. https://doi.org/10.1785/0220220193

Trugman, D. T., & Shearer, P. M. (2017). GrowClust: A hierarchical clustering algorithm for relative earthquake relocation, with application to the Spanish springs and Sheldon, Nevada, earthquake sequences. *Seismological Research Letters*, *88*(2A), 379–391. https://doi.org/10.1785/0220160188

Tuffen, H., Smith, R., & Sammonds, P. R. (2008). Evidence for seismogenic fracture of silicic magma. *Nature*, *453*(7194), 511–514. https://doi.org/10.1038/nature06989

Ulberg, C. W., Creager, K. C., Moran, S. C., Abers, G. A., Thelen, W. A., Levander, A., et al. (2020). Local source *Vp* and *Vs* tomography in the Mount St. Helens Region with the iMUSH Broadband array. *Geochemistry, Geophysics, Geosystems*, *21*(3), e2019GC008888. https://doi.org/10.1029/2019GC008888

University of Washington. (1963). Pacific Northwest seismic network - University of Washington [Dataset]. *International Federation of Digital Seismograph Networks*. https://doi.org/10.7914/SN/UW

USGS. (2023). Volcano updates. Cascades volcano observatory information statement Monday. Retrieved from https://www.usgs.gov/volcanoes/mount-st.-helens/volcano-updates

Vidale, J. E., Schmidt, D. A., Malone, S. D., Hotovec-Ellis, A. J., Moran, S. C., Creager, K. C., & Houston, H. (2014). Deep long-period earthquakes west of the volcanic arc in Oregon: Evidence of serpentine dehydration in the fore-arc mantle wedge. *Geophysical Research Letters*, *41*(2), 370–376. https://doi.org/10.1002/2013GL059118

Waite, G. P., Chouet, B. A., & Dawson, P. B. (2008). Eruption dynamics at Mount St. Helens imaged from broadband seismic waveforms: Interaction of the shallow magmatic and hydrothermal systems. *Journal of Geophysical Research*, *113*(B2), 2007JB005259. https://doi.org/10.1029/2007JB005259

Waite, G. P., & Moran, S. C. (2009). VP structure of Mount St. Helens, Washington, USA, imaged with local earthquake tomography. *Journal of Volcanology and Geothermal Research*, *182*(1–2), 113–122. https://doi.org/10.1016/j.jvolgeores.2009.02.009

Wang, W., Shearer, P. M., Vidale, J. E., Xu, X., Trugman, D. T., & Fialko, Y. (2022). Tidal modulation of seismicity at the Coso geothermal field. *Earth and Planetary Science Letters*, *579*, 117335. https://doi.org/10.1016/j.epsl.2021.117335

Wanke, M., Karakas, O., & Bachmann, O. (2019). The genesis of arc dacites: The case of Mount St. Helens, WA. *Contributions to Mineralogy and Petrology*, *174*(1), 7. https://doi.org/10.1007/s00410-018-1542-6

Warren, N. W., & Latham, G. V. (1970). An experimental study of thermally induced microfracturing and its relation to volcanic seismicity. *Journal of Geophysical Research*, *75*(23), 4455–4464. https://doi.org/10.1029/JB075i023p04455

Weaver, C. S., Zollweg, J. E., & Malone, S. D. (1983). Deep earthquakes beneath Mount St. Helens: Evidence for magmatic gas transport? *Science*, *221*(4618), 1391–1394. https://doi.org/10.1126/science.221.4618.1391

Wech, A. G., Thelen, W. A., & Thomas, A. M. (2020). Deep long-period earthquakes generated by second boiling beneath Mauna Kea volcano. *Science*, *368*(6492), 775–779. https://doi.org/10.1126/science.aba4798

White, R. A., & McCausland, W. A. (2019). A process-based model of pre-eruption seismicity patterns and its use for eruption forecasting at dormant stratovolcanoes. *Journal of Volcanology and Geothermal Research*, *382*, 267–297. https://doi.org/10.1016/j.jvolgeores.2019.03.004

Wiemer, S., & Wyss, M. (2000). Minimum magnitude of complete reporting in earthquake catalogs: Examples from Alaska, the western United States, and Japan. *BSSA*, *90*, 859–869. https://doi.org/10.1785/0119990114

Wong, Y., & Segall, P. (2019). Numerical analysis of time-dependent conduit magma flow in dome-forming eruptions with application to Mount St. Helens 2004–2008. *Journal of Geophysical Research: Solid Earth*, *124*(11), 11251–11273. https://doi.org/10.1029/2019JB017585

Wong, Y., & Segall, P. (2020). Joint inversions of ground deformation, extrusion flux, and gas emissions using physics-based models for the Mount St. Helens 2004–2008 eruption. *Geochemistry, Geophysics, Geosystems*, *21*(12), e2020GC009343. https://doi.org/10.1029/2020GC009343

Wong, Y., Segall, P., Bradley, A., & Anderson, K. (2017). Constraining the magmatic system at Mount St. Helens (2004–2008) using bayesian inversion with physics-based models including gas escape and crystallization. *Journal of Geophysical Research: Solid Earth*, *122*(10), 7789–7812. https://doi.org/10.1002/2017JB014343

Zhang, H., Glasgow, M., Schmandt, B., Thelen, W. A., Moran, S. C., & Thomas, A. M. (2022). Revisiting the depth distribution of seismicity before and after the 2004–2008 eruption of Mount St. Helens. *Journal of Volcanology and Geothermal Research*, *430*, 107629. https://doi.org/10.1016/j.jvolgeores.2022.107629

References From the Supporting Information

Cao, A., & Gao, S. S. (2002). Temporal variation of seismic *b*-values beneath North Eastern Japan island arc. *Geophysical Research Letters*, *29*(9). https://doi.org/10.1029/2001GL013775

Fischler, M. A., & Bolles, R. C. (1981). Random sample consensus: A paradigm for model fitting with applications to image analysis and automated cartography. *Communications of the ACM*, *24*(6), 381–395. https://doi.org/10.1145/358669.358692

Huber, P. J. (1964). Robust estimation of a location parameter. *The Annals of Mathematical Statistics*, *35*(1), 73–101. https://doi.org/10.1214/aoms/1177703732

Lomax, A., & Henry, P. (2023). Major California faults are smooth across multiple scales at seismogenic depth. *Seismica*, *2*(1). https://doi.org/10.26443/seismica.v2i1.324

Murray, J. R., & Svarc, J. (2017). Global positioning system data collection, processing, and analysis conducted by the U.S. geological survey earthquake hazards program. *Seismological Research Letters*, *88*(3), 916–925. https://doi.org/10.1785/0220160204

Pedregosa, F., Varoquaux, G., Gramfort, A., Michel, V., Thirion, B., Grisel, O., et al. (2011). Scikit-learn: Machine learning in python. *Journal of Machine Learning Research*, *12*, 2825–2830. http://jmlr.org/papers/v12/pedregosa11a.html

Prieto, G. A. (2022). The multitaper spectrum analysis package in python. *Seismological Research Letters*, *93*(3), 1922–1929. https://doi.org/10.1785/0220210332